1. Introduction and aim of study

The platinum-group elements (PGE - Ru, Rh, Pd, Os, Ir, and Pt) are often considered to be strongly siderophile and geochemically coherent (Fleet and Stone, 1991; Schmitt *et al.*, 1989). PGE patterns in undepleted mantle xenoliths (lherzolites and peridotites) compared to chondrites show relatively uniform depletion of the PGE during the primary differentiation of planetary material (Barnes *et al.*, 1985; Walker *et al.*, 1996). However, numerous natural examples of fractionation and preferential concentration of PGE have been recorded through the years. Palme and Wlotzka (1976) reported extreme enrichment of Os, Ir, Ru, Rh and Pt in metallic and sulphide phases in refractory inclusions in C3V chondritic meteorites, while fractionation of PGE during geological processes is shown by the substantial enrichment of Rh, Pd and Pt compared to Os, Ir and Ru in crustal mafic intrusions (Naldrett *et al.*, 1979; Naldrett, 1981). In contrast, deposits related to ultramafic rocks (komatiites) characteristically have comparatively much lower contents of Rh, Pd and Pt compared to Os, Ir and Ru. Enrichment of Os, Ir and Ru in ophiolites in chromitites (Page and Talkington, 1984; Barnes *et al.*, 1985; Legendre and Auge, 1986; Walker *et al.*, 1996) can be attributed to partial melting of mantle material, which results in a residue rich in the refractory elements Os, Ir and Ru (concentrated in the chromitite) and a melt enriched in Rh, Pd and Pt, depending on the S saturation of the source. This melt could then form the cumulate upper portions of the ophiolite which are enriched in Rh, Pd and Pt (Page and Talkington, 1984). During partial melting of peridotites, Pt and Pd are mobilised with Cu, while Ir and Ru are refractory, and the behaviour of Rh varies (Gueddari *et al.*, 1996; Pattou *et al.*, 1996). Cu-rich sulphide ores are characteristically enriched in Pt, Pd and Au, and depleted in Os, Ir, Ru and Rh compared to spatially-related Ni ores (Naldrett *et al.*, 1982; Naldrett, 1989; Barnes *et al.*, 1997). This latter enrichment is believed to be the result of equilibrium partitioning during fractional crystallisation of a sulphide melt and its change into a more Cu-rich residual liquid.

All these fractionation processes are controlled by the partition coefficients of the PGE between various phases, and can be characterised by these coefficients. A partition or distribution coefficient (D) is the ratio of the content of an element in two co-existing

phases: for example the ratio of the Pt content in metal, measured in wt%, to Pt content in co-existing sulphide. Exact knowledge of partition coefficients provides quantitative data necessary to evaluate precious metal behaviour in high temperature magmatic processes in nature, as well as in technical processes such as smelting and refining. Their application allows a better understanding of the chemistry of these trace elements in metal-matte systems in metallurgical practice (Schlitt and Richards, 1975).

The phases in which PGE most frequently occur in nature consist of base-metal sulphides, mainly Cu, Fe and Ni sulphides, so that the PGE are normally extracted and refined together with these and a large range of minor elements. The simplified Cu-Fe-Ni-S system is already very complex, and to fully understand and to permit prediction of the behaviour of the PGE in such complex systems, their behaviour in binary and ternary systems needs to be known. Potential developments in the beneficiation of PGE may involve further reduction of the S-contents in the mattes compared to present practice. Presently alloys of varying composition (Cu-Ni±Fe) are formed during slow cooling, but the behaviour of PGE in the systems Cu-S, Ni-S and Fe-S are poorly understood. Although a fair amount of research has been published on the more complex systems resembling natural conditions (e.g. Fleet *et al.*,1993, Li *et al.*, 1996, Barnes *et al.*, 1997), very little information is available on the partitioning of PGE in the binary and ternary systems. It was therefore decided to quantify the partitioning of Rh, Pd and Pt between the metals and selected sulphide phases and melt compositions in the Ni-S, Cu-S and Fe-S systems. Due to insurmountable technical problems that were experienced in the investigation of the Fe-S system (discussed in detail in section 5.3.), this system was not investigated as comprehensively as the other systems.

1.1. Choice of PGE contents for investigation

The aim of this investigation set out as the determination of the behaviour of PGE at trace concentrations, comparable to typical PGE matte contents, and higher than natural concentrations, in the Cu-Fe-Ni-S system. The concentrations of PGE in nature are very low (e.g. Barnes *et al.*, 1985) and, although somewhat higher in metallurgical mattes (e.g. Schlitt and Richards, 1975), they still occur in trace amounts. Stone *et al.* (1990) underlined the

importance of trying to keep experimental conditions as close as possible to the conditions to which the results would be applied. Initial experiments were prepared to contain 500 ppm, 1000 ppm and 2000 ppm PGE. Although these concentrations are higher than typical PGE contents in nature, and somewhat high for metallurgical comparison, they were chosen because quantitative analyses would still be practical.

To determine if interpolation and extrapolation of partition coefficients from low to much higher PGE concentrations would be meaningful, additional experiments with PGE contents of 6000 ppm and 10000 ppm were prepared. Jones and Drake (1983) and Willis and Goldstein (1982) observed that the Ni partition coefficient in the Fe-Ni-S system (with minor impurities) is influenced by the bulk Ni content of the system. Crocket *et al.* (1997), in an investigation of PGE partitioning between sulphide and basalt melt, reported that variation of partition coefficients for some PGE was related to initial PGE concentration in charges. Barnes *et al.* (1997), however, compared their partition coefficients, calculated from experiments performed with PGE at percent levels, with experiments reported in the literature where PGE contents were at ppm levels and found no significant difference. The investigation of PGE partitioning in this study using at least three different PGE concentrations makes it possible to determine whether the partition coefficient of a specific PGE remains constant from low to high concentrations.

To determine how the presence of other PGE influence the partitioning behaviour of a single PGE, each PGE was investigated in the absence of other PGE, as well as in combination with them. Sulphur content in liquid was found to influence the partition coefficients of siderophile elements, such as Ir (Jones and Drake, 1983), and Schlitt and Richards (1975) determined that in the region of liquid immiscibility in the Cu-Ni-S system, an increase in Ni content caused a systematic change in the Ag partition coefficient between alloy and melt. The influence of PGE on each other was not expected to be as severe as in these examples.

Considering that each PGE would be investigated at at least three different concentrations at a chosen bulk composition, as well as isolated from other PGE, it was considered

impractical to include all six PGE in the investigation. Rh, Pd and Pt were chosen, as these are economically the most important PGE. Furthermore, Pt is a heavy PGE, while Rh and Pd are light PGE, and Pt and Pd traditionally behave similarly in mss systems as opposed to Rh.

1.2. Choice of major element compositions of experiments

1.2.1. The Ni-S system at low S contents

Kullerud and Yund (1962) reviewed all the previous work on the binary system Ni-S and discussed a low temperature Ni_7S_6 phase that transforms to a high temperature Ni_7S_6 phase. Further research by Kulagov *et al.* (1969), Naldrett *et al.* (1972) and Fleet (1987, 1988) established that stoichiometrically and structurally, low temperature Ni_9S_8 (godlevskite) was the low temperature Ni_7S_6 phase of Kullerud and Yund (1962). Godlevskite occurs at temperatures below that of interest to the present investigation.

The thermodynamic properties and phase relations of the system Ni-S were also studied by Lin *et al.* (1978), Sharma and Chang (1980) and Cemic and Kleppa (1986). Except for native Ni, five mineral phases are now known to exist within the Ni-S system: heazlewoodite (Ni_3S_2), godlevskite (Ni_9S_8 - see above), millerite (NiS), polydymite (Ni_3S_4) and vaesite (NiS_2). Additionally, high temperature modifications are known for Ni_3S_2 (above 533°C), Ni_9S_8 (above 397°C) and NiS (above 282°C) (Sharma and Chang, 1980). Of all these phases, only heazlewoodite is commonly found in slow-cooled metallurgical mattes, which are relatively low in sulphur.

The phase diagrams by Sharma and Chang (1980) and Cemic and Kleppa (1986) were used to determine the bulk compositions of experimental charges. All experiments were designed to contain co-existing nickel and sulphide melt. The charges were equilibrated from 1200°C to 700°C, at 100°C intervals. The weight percentages of elements in the experimental charges are given in the Appendix, Tables A1 to A6.

1.2.2. The Cu-S system at low S contents

The phase relations and compositions of the Cu-S system have been investigated by a number of authors; the most relevant publications include Kullerud (1960), Morimoto and Gyobu (1971), Schlitt and Richards (1973) and Chakrabarti and Laughlin (1986).

Bulk compositions for experimental charges were determined based on the phase diagram by Chakrabarti and Laughlin (1986). Experiments were designed from 1200°C to 700°C at 100°C intervals, at compositions which would allow the investigation of co-existing copper and digenite, co-existing Cu-rich melt and digenite, co-existing digenite and S-rich melt, and immiscible Cu-rich melt and S-rich melt. Weight percentages of elements in the experimental charges are given in the Appendix, Tables A7 to A12.

1.2.3. The Fe-S system at low S contents

The phase diagrams by Kullerud and Yoder (1959), Kullerud (1961), Chuang *et al.* (1985), supported by the later phase diagram by Fleet and Stone (1991), were used to determine the bulk major element compositions of the experimental charges for the investigation of this system. Experiments were designed from 1200°C to 700°C at 100°C intervals, at compositions that would contain co-existing iron and troilite, co-existing iron and quenched melt, and co-existing pyrrhotite and quenched melt. Weight percentages of elements in the experimental charges are given in the Appendix, Tables A13 to A18.

1.3. Previous investigations of PGE partition coefficients

1.3.1. The Ni-S system

Urban *et al.* (1995) investigated three nickel-sulphide buttons obtained from different nickel sulphide fire-assay extraction methods, containing traces of PGE. Heazlewoodite (Ni_3S_2) was the dominant phase, with lesser PGE-sulphides and PGE-Ni alloys. It was found that Rh, and to a lesser degree Ru, display a strong affinity for the PGE-sulphides (with

differing compositions in different buttons), with PGE sulphide / heazlewoodite partition coefficients between 25 and 55. The authors suggested that the same behaviour could be expected for Pd. Ir, Os and Pt tend to alloy with each other and Ni, with metal / heazlewoodite and metal / PGE-sulphide partition coefficients in the order of 500 to 1000 for Ir, 100 to 400 for Os and 100 to 1000 for Pt.

1.3.2. The Cu-S system

Gerlach *et al.* (1972) investigated the partitioning of Pt and Au at 1200°C in several systems, including the Cu-S system, and determined a D_{Pt} of 2000 for Cu / Cu sulphide. Schlitt and Richards (1975) determined an experimental D_{Pd} of 167 and D_{Pt} of 2500 at 1200°C. Taylor (1983) investigated the thermodynamics involved in the partitioning of trace elements between Cu bullion (99 % Cu) and Cu matte (roughly Cu_2S), using experiments equilibrated at 1200°C. He found a D_{Rh} of 110 from the experiments, and calculated D's of 11 for Rh, 25 for Pd, 550 for Ru, 5400 for Ir, and 6800 for Pt. He also quoted D's of 70 for Ru (Romanov *et al.*, 1973), 80 for Pd (Burylev *et al.*, 1974), 340 for Ir (Romanov *et al.*, 1973) and 2000 for Pt (Burylev *et al.*, 1974).

1.3.3. The Fe-S system

The classical study by Noddack *et al.* (1940) on partitioning of minor amounts of PGE between iron and sulphide are now known to be suspect due to impure separation of the phases (Fleet and Stone, 1991). Partition coefficients for the iron and sulphide liquid at 1300°C to 985°C were about 8 to 13 for Ru, Rh, Os, Ir and Pt, and 2.6 for Pd, with all PGE preferring the iron. For iron and FeS at 985°C, the partition coefficients for all six PGE were found to be between 10 and 16 (all PGE preferring iron). Analyses were performed on bulk mechanical separates, and the FeS is now known to have contained about 6 wt% iron, which influenced the calculated D's.

Jones *et al.* (1986) reported an iron / troilite partition coefficient of 150 for Pd, and Jones and Drake (1986) an iron / sulphide partition coefficient of 83 for Ir.

The investigation by Fleet and Stone (1991) on the Fe-Ni-S system contained very low contents of Ni, with some experiments containing no Ni at all, so that these results are applicable to the Fe-S system. In co-existing iron and sulphide liquid assemblages, Os, Ir and Pt were reported to be concentrated in the alloy phases (strongly siderophile), with Pd less so. Alloy / sulphide liquid partition coefficients reported for 1000°C are 1 to 2 for Pd, 30 to 110 for Rh and >1000 for Os, Ir, Pt and Ru. In co-existing troilite and sulphide liquid assemblages Ru, and to a lesser degree Rh, are the only PGE with a significant solubility for troilite, while Pd partitions strongly into the liquid, confirming the minimal substitution of PGE in stoichiometric troilite.

Chabot and Drake (1997) experimentally investigated the metal / liquid D for Pd along with Ag. D_{Pd} changed from slightly incompatible in metal to slightly compatible (0.5 to 2), as the S content of the liquid increased.

1.3.4. The Fe-Ni-S system

Fleet and Stone (1991) investigated the partitioning of minor amounts of all six PGE in the Fe-Ni-S system at 1000°C to 1400°C at low pressure. They reported distinctly different partitioning behaviour for the light and heavy PGE. Os, Ir and Pt are preferentially concentrated into the alloy phases, while Pd is depleted in alloys and relatively enriched in sulphide liquid. Pd varies from siderophile to chalcophile in assemblages with Fe-containing alloy, but is chalcophile in all other alloy-containing assemblages. The reported partition coefficients for Fe alloy / sulphide liquid are 1 - 2 for Pd (comparable to Ni), 30 - 110 for Rh, and >1000 for Pt, Ir and Os. The overall affinity for Fe-rich alloy is Os >> Ir > Pt > Ru > Rh >> Pd. Ru, and to a lesser extent Rh, are the only PGE with significant solubility in troilite co-existing with sulphide melt, while Pd partitions strongly into the melt. Minor amounts of Ru, Rh and Pd were reported in Ni-bearing troilite.

Distler *et al.* (1977) investigated the distribution of Ru, Rh and Pd between pyrrhotite, pentlandite and sulphide melt, again observing enrichment of Pd in the melt, while Ru and Rh partitioned into co-existing sulphide.

The partitioning of minor amounts of Ir in the Fe-Ni-S system was investigated by Willis and Goldstein (1982) and Jones and Drake (1983), who found the D_{Ir} to be dependent on the S content in the liquid. Jones and Drake (1986) adopted an Fe-rich alloy / sulphide liquid partition coefficient of 83 for Ir, and Jones and Malvin (1990) constructed a positive linear relationship between the S content in the liquid and the Ir partition coefficient in solid metal.

Fleet *et al.* (1999) investigated the partitioning of PGE and Au between solid metal and liquid metal sulphide, and reported high solid metal / liquid metal partition coefficients for the most refractory metals (D_{Os}: 249 to 6180, D_{Ir}: 367 to 4180), intermediate for Ru (41 to 164) and Pt (40 to 300), and near unity for the least refractory metals (D_{Pd}: 0.7 to 1.47, D_{Ni}: 1.40 to 2.77, D_{Au}: 1.32 to 3.87). They report variation in bulk composition as the most important cause for the variation in the partition coefficients.

1.3.5. The Cu-Fe-Ni-S system

Many nickel-copper sulphide ore bodies contain Cu-rich and Fe-rich portions, with the Fe-rich ore typically enriched in Os, Ir, Ru and Rh, and the Cu-rich ore enriched in Pt, Pd and Au (Li and Barnes, 1996; Barnes *et al.*, 1997). The Fe-rich ore represents the first phase to crystallise from a sulphide melt - the monosulphide solid solution (mss), while the Cu-rich ore represents the fractionated liquid. Fleet *et al.* (1993) crystallised mss from Cu- and Ni-enriched sulphide liquid at 1000 – 1040°C, and determined partition coefficients (weight % metal in mss / weight % metal in sulphide liquid) of 4.3 for Os, 3.6 for Ir, 4.2 for Ru, 3.0 for Rh, 0.21 for Pt and 0.21 for Pd. Barnes *et al.* (1997) reported D_{Pd}: 0.005 to 0.435, D_{Rh}: 0.045 to 7.43, D_{Pt}: 0.013 to 0.46 and D_{Ir}: 0.429 to 17, depending on temperature and S content. Barnes *et al.* (1994) and Li *et al.* (1996) found D_{Pd}: 0.14, D_{Pt}: 0.1, and D_{Rh}: 4 to 7. For their low fS_2 experiments they found D_{Pd}: 0.02 and D_{Rh}: 0.3 to 0.4, comparable to the

low fS_2 partition coefficients by Fleet and Stone (1991) of D_{Pd}: 0.02 and D_{Rh}: 0.2 to 0.3. According to Peregoedova (1997), the most important difference between Pt and Pd behaviour during crystallisation of Cu-Fe-Ni-S melt is that Pt tends to form its own compounds, including sulphides at high fS_2, whereas Pd prefers (Fe,Ni,Cu)-sulphide solid-solutions.

1.3.6. Other relevant systems

1.3.6.1. Pd-Fe-S system

Makovicky *et al.* (1986), Makovicky *et al.* (1988) and Makovicky and Karup-Møller (1993) investigated this system. S-rich pyrrhotite dissolved more than 12 wt% Pd while troilite contained no detectable Pd at 900°C. At 500°C Pd in troilite was below detection, up to 0.5 wt% Pd was measured in S-rich pyrrhotite, and less than 0.01 wt% Pd measured in pyrite. Previous research in this system is recorded in publications by Skinner *et al.* (1976), Distler (1980) and Bryukvin *et al.* (1985).

1.3.6.2. Pt-Fe-S system

At 900°C up to 2.2 wt% Pt was measured in S-rich pyrrhotite, and Pt in troilite was below detection (Makovicky *et al.*, 1986). Pt-rich pyrrhotite was found to co-exist with PtS and PtS_2. At 500°C Pt was below detection in pyrrhotite of all compositions and pyrite.

1.3.6.3. Rh-Fe-S system

It was found that pyrrhotite can contain up to 44 wt% Rh at 900°C, while still retaining its essential X-ray characteristics (Makovicky *et al.*, 1986). At 500°C, up to 6.7 wt% Rh was found in pyrrhotite, which decreased to around 1.1 wt% Rh at lower S contents. Rh in pyrite was below detection.

1.3.6.4. Pd-Ni-S system

This system was investigated by Karup-Møller and Makovicky (1993). They found that at 900°C up to 4.9 wt% Pd was present in $Ni_{1-x}S$, and up to 2.1 wt% Pd in NiS_2. At 725°C they detected up to 2.6 wt% Pd in $Ni_{1-x}S$, 4.3 wt% Pd in Ni_3S_2 and 1.0 wt% Pd in NiS_2. At 500°C $Ni_{1-x}S$ contained up to 0.5 wt% Pd, Ni_3S_2 up to 13.7 wt% Pd, Ni_7S_6 up to 1.1 wt% Pd and NiS_2 up to 0.3 wt% Pd. Pd in $Ni_{1-x}S$ and NiS_2 was below detection at 400°C, while up to 0.4 wt% Pd was detected in Ni_3S_2, and up to 0.2 wt% Pd in Ni_7S_6.

1.3.6.5. Cu-Pd-S system

Karup-Møller and Makovicky (1999) investigated this system at 900°C, 725°C, 550°C and 400°C. $Cu_{2-x}S$ dissolved up to 0.7 at% Pd at 900°C and up to 0.9 at% Pd at 725°C, but at 550°C Pd was below detection in $Cu_{2-x}S$, and at 400°C Pd was below detection in both $Cu_{2-x}S$ and CuS.

1.3.6.6. Cu-Rh-S system

This system was investigated at 900°C, 725°C and 500°C by Makovicky and Karup-Møller (1994). At 900°C $Cu_{2-x}S$ was found to contain up to 0.04 at% Rh, while containing only traces of Rh at lower temperatures. Rh in CuS at 500°C was also below detection. Copper metal was found to contain up to 10 at% Rh at all temperatures.

1.3.6.7. Fe-Ni-PGE systems

Blum *et al.* (1989) investigated phase boundaries and tie lines in the Fe-Ni-Ru system at 1000°C, 800°C and 600°C, as well as the partitioning behaviour of Pt and Ir between phases in this system. Pt was found to be more compatible with face-centred cubic Ni-Fe alloy, while Ir was more compatible with close-packed hexagonal Ru-Fe alloy, even though pure Pt and Ir both have face-centred cubic crystal structures.

1.3.6.8. Fe-Ni-PGE-S system

The Fe-Ni-PGE-S system was investigated at 500°C by Makovicky *et al.* (1986). No Pt, but up to 12.5 wt% Pd and up to 12.4 wt% Rh was detected in pentlandite. It was concluded that Pd and Rh, along with Ru, can fully occupy the octahedral metal positions in pentlandite, while Pt cannot enter the pentlandite structure. It was also observed that at low fS_2 PGE prefer alloy with Fe to troilite. With moderate increase in fS_2 the solubility of Rh in pyrrhotite increased sharply.

The Pd-Fe-Ni-S system was investigated by Distler *et al.* (1977). Makovicky and Karup-Møller (1995) and Makovicky *et al.* (1990) experimentally investigated the systems Fe-Ni-Pd-S and Fe-Pt-Pd-As-S.

2. Experimental technique

2.1. Sealed quartz glass tube technique

This technique was described by Kullerud (1971) and was also used for experimental work by Bruwer (1996) in the experimental sulphide laboratory of the Geology Department at the University of Pretoria. Experiments were carried out in high purity quartz glass tubes. Pure SiO_2 does not react with sulphur or the relevant metals at the temperatures under investigation, making it a suitable, as well as affordable, container for this type of investigation. The walls of the tubes have to be thick enough to withstand high S pressure from the inside during heating, but also thin enough to allow for very fast cooling of the contents during quenching. In this study, all quartz glass tubes used had an inside diameter of 4 mm and a wall thickness of 1 mm.

One end of a short tube (usually between 8 and 10 cm - Figure 1A) was heated over a natural gas - oxygen flame until it softened and melted to form a closed end (Figure 1B). To ensure that no contaminants were present in the tube, it was then thoroughly cleaned. Contaminants would have influenced the experiments, or reacted with quartz at high temperatures to weaken the glass. The tube was rinsed with cleaning solution (Extran), followed by thorough rinsing with clean water, and lastly rinsing with acetone to reduce the amount of static electricity built-up during later weighing-in of the powders. Static electricity was observed to cause the powders to cling to the walls of the tube, so that not all the reactants would reach the bottom where reactions and equilibration take place. When the tube was dry, the starting materials were weighed in (Figure 1C). A short quartz glass rod, with a diameter of slightly less than 4 mm and a length of about 2 cm, was placed on top of the contents in the tube (Figure 1D). The open end of the tube was then connected to a vacuum pump and the system evacuated down to between 10 and 60 milliTorr (1.3 to 8 Pa). During evacuation the rod reduced the volume in the tube to allow faster evacuation, and protected the contents of the tube by partly blocking the opening of the tube, preventing the powder inside from being sucked out. A wet cloth was wrapped around the bottom end of the tube where the experimental charge was located. The tube was then heated in the gas

flame at a position above the rod (Figure 2), rotated evenly while remaining under vacuum until the tube wall collapsed on the rod and sealed the contents of the tube (Figure 1E). The wet cloth protected the charge from the heat during this process.

2.2. Starting material

Fe, Cu and Ni with purity of ≥ 99.98% and S with purity of at least 99.99% were used for all experiments, as well as specpure Pt, Pd and Rh.

Before the elements were weighed in, Cu and Ni were reduced to eliminate all oxygen that might have been introduced through surface oxidation. The reduction process is illustrated in Figure 3. A tube furnace was fitted with a quartz glass tube. One end of the tube was connected to a H_2 and Ar gas inlet, and the other end to a rubber tube which was led through a beaker filled with water. No openings were left where atmospheric gases could infiltrate the system. Powder of the pure element was placed in a quartz glass boat and inserted into the tube in the tube furnace. The powder was then heated at 600°C for 6 hours in an atmosphere of H_2 and Ar gas. The gas entered the tube through the inlet, and exited on the other end, where the pressure of the gases could be monitored by checking the speed of the gas bubbles as they rose through the water. After six hours the elements were allowed to cool in an Ar atmosphere, before they were removed from the tube. The elements usually had to be crushed, sometimes in acetone to prevent oxidation as best as possible, before they could be weighed into the tubes. The reduction process was performed immediately before the elements were weighed into the tubes, to limit oxidation as much as possible.

The reduction technique described above was found to be ineffective for Fe. An abnormally high number of the Fe-containing experiments failed and were oxidised. This is believed to be due to oxidation of the Fe after reduction and before weighing-in, resulting in FeO formation and reaction with the quartz glass. Consequently, reduced Fe was first weighed into tubes, and these tubes were again heated in the tube furnace under Ar + H_2 atmosphere (Figure 4). After reduction, S and PGE were weighed in and the tube sealed as quickly as possible. The weight difference before and after reduction due to oxygen loss was found to

be approximately 0.5 wt% (~0.002 g loss from 0.400 g). The Fe weight after reduction was used to calculate the amount of S and PGE to be added. Different reduction times, temperatures and H_2 pressures were evaluated to determine a possible effect on the success of the experiments, but no clear conclusions could be drawn. The higher success rate achieved for later experiments could be the result of reduction of Fe after weighing-in, allowing much less time for the Fe to oxidise. However, experience obtained through the preparation of hundreds of experiments in the laboratory suggests that quality differences exist between quartz tube batches, which led to many cracked tubes even in Fe-free experiments.

Sulphur was dried at 95°C and stored in a desiccator.

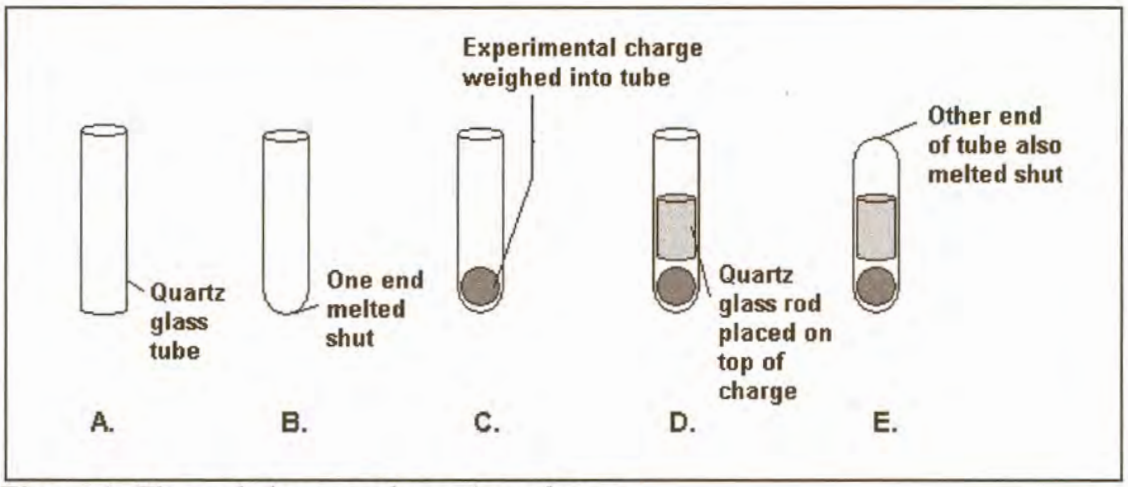

Figure 1. *The sealed quartz glass tube technique.*

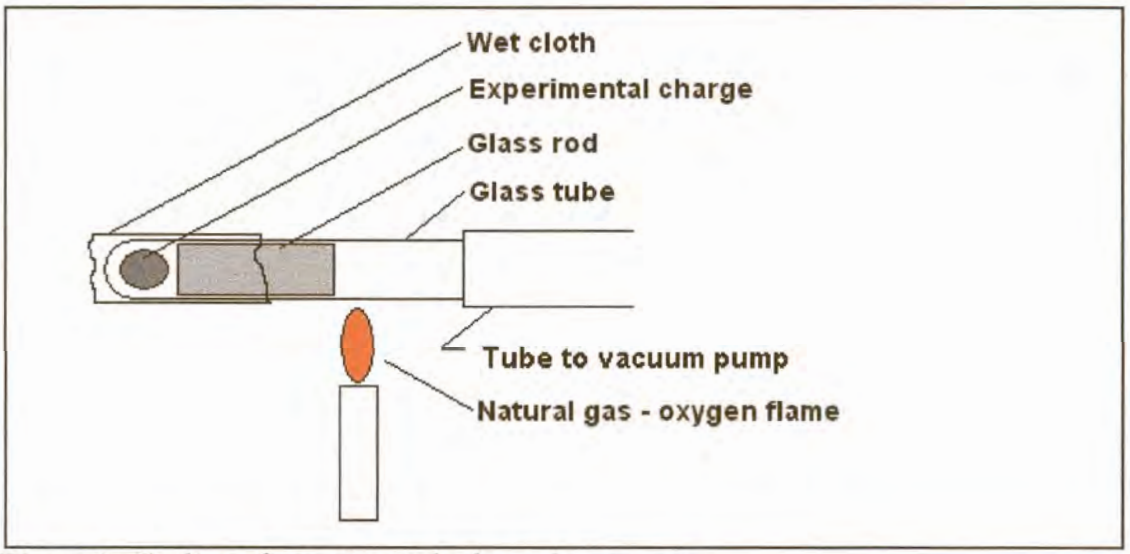

Figure 2. *Sealing of experimental tube under vacuum.*

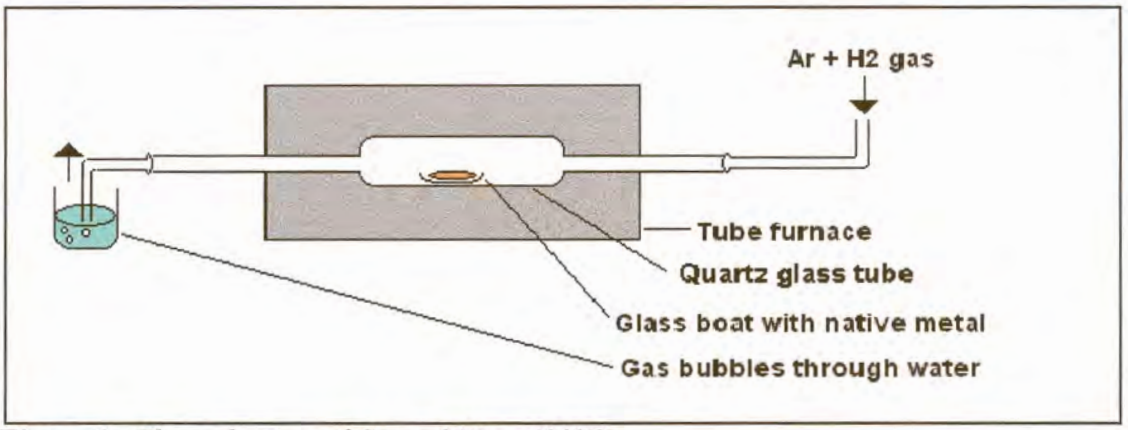

Figure 3. *The reduction of Cu and Ni at 600°C.*

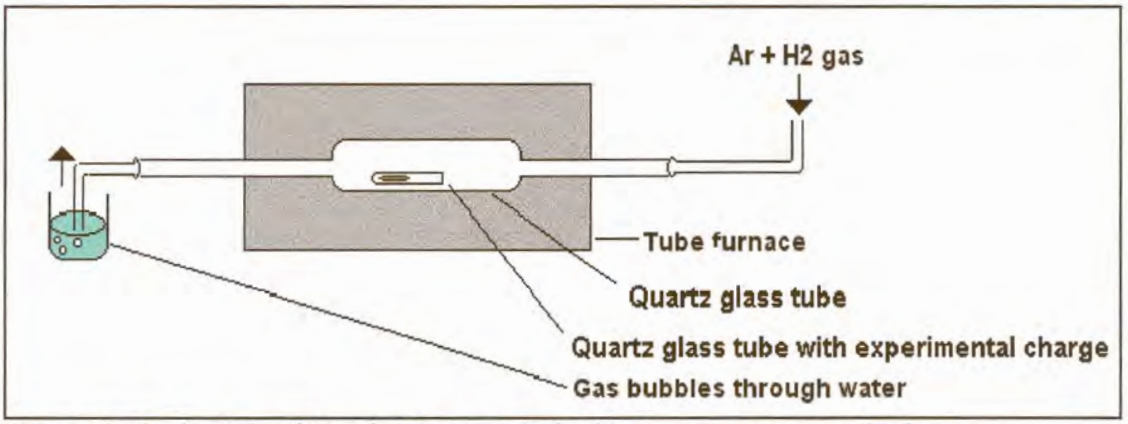

Figure 4. *Reduction of Fe after being weighed into an experimental tube.*

Very low concentrations of PGE were investigated. To be able to accurately weigh 500 ppm of PGE into an experiment, charges with a total weight of 2 grams had to be prepared. The 2 gram Fe-S experiments proved very difficult to prepare, as both Fe and S are light and the length of 2 grams of material weighed into a 4 mm diameter tube was about 20 cm. To obtain proper equilibration along the entire length of the tube was very difficult. These long tubes also cracked very easily, and the contents always separated during reaction. Experimental charges of 1 gram were prepared to investigate PGE contents of 1000 ppm, and 0.5 gram charges were prepared to investigate higher PGE contents. All the experimental charges prepared to investigate the Cu-S, Ni-S and Fe-S assemblages at all temperatures are shown in the Appendix, Tables A1 to A18.

2.3. Equilibration of experiments

2.3.1. Pre-reaction

After the tubes were sealed, they were heated in a pre-reaction furnace at 700°C to 800°C for at least one day. This allowed the pure sulphur powder to react with the metals, which prevented explosion of the tubes due to high sulphur vapour pressure at higher temperatures. According to Kullerud and Yoder (1959), pure sulphur pressure is between 15 and 35 bar at 700°C to 800°C. Sulphur pressure increases logarithmically with increasing temperature, and at higher temperatures pure sulphur pressure would crack the quartz glass tubes very easily. By pre-reacting the experiments at low temperatures, the presence of pure sulphur inside the tubes at higher temperatures was avoided.

2.3.2. Equilibration

Two large chamber furnaces, each fitted with six horizontal tubes reaching from the front door to the back of the furnace, were used for equilibration at the desired temperatures (Figure 5A). The temperature gradients along the length of the tubes were measured with a calibrated thermocouple. An experimental charge was inserted horizontally into one of the tubes and left at a position where the desired temperature was measured before and during equilibration over the entire length of the charge. A thermally isolating plug was inserted into the open front end of the tube to prevent heat loss. When the temperature in a tube was measured, a plug with a small hole was placed into the front end of the tube, and a calibrated hand-held thermocouple was inserted through this hole (Figure 5B). The temperature around the charge was considered unacceptable if it varied by more than 2°C from the desired temperature. Some of the lower-temperature experiments were placed vertically in holders and reacted in a smaller chamber furnace. A thermocouple was inserted through a small hole in the door of the furnace to ensure that the reaction temperature was satisfactory. When not used, the hole was filled with thermally isolating material.

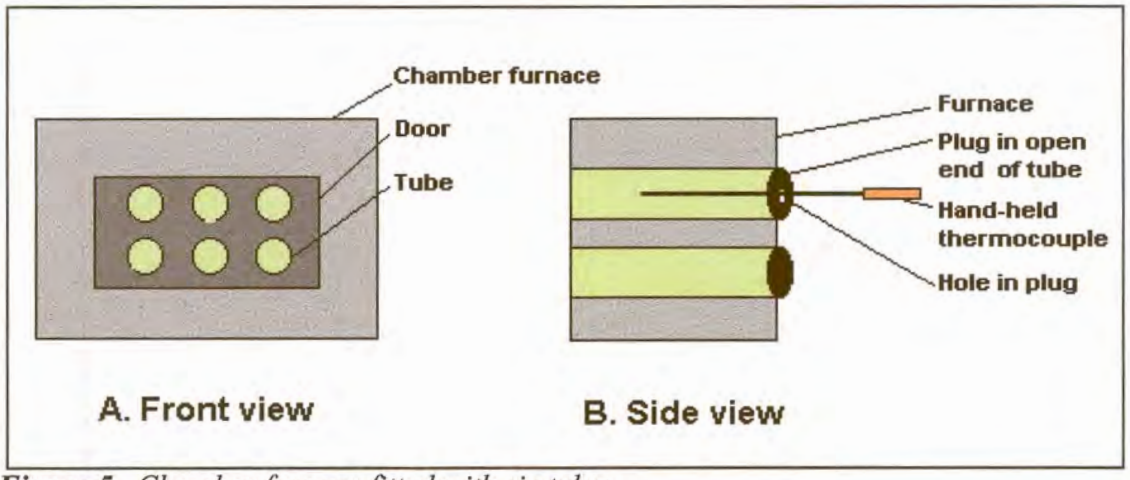

Figure 5. *Chamber furnace fitted with six tubes.*

All the experiments in this investigation were reacted at temperatures between 1200°C and 700°C. The high temperature experiments reached equilibrium much faster than the low temperature experiments, and were removed from the furnace after shorter time periods. Lengthy exposure of quartz glass to high temperatures (~1200°C) results in recrystallisation and weakening of the tubes. When these experiments were exposed to the higher temperatures for long time periods, the tubes tended to crack, which resulted in oxidation of the charges in the furnace, or cracking of the tubes when the experiments were quenched.

2.3.3. Quenching

When the charges were assumed to have reached equilibrium, they were quenched. As sulphide liquid crystallises into lower temperature phases during quenching, it is of great importance to cool the charge as fast as possible to limit the crystallisation time and therefore the crystallite sizes. A tall cylinder filled with cooled water was placed at the open end of a furnace tube, and the charge was then dropped into the cylinder and allowed to fall through the water, in this way preventing the formation of a heated or isolating boundary layer. Other cooling mediums that were tested by Bruwer (1996) were water and ice, supercooled brine and liquid nitrogen, but no systematic improvement on the quenching speed was observed. It is believed that the low thermal conductivity of the quartz glass limits the quenching speed more than the quenching medium does. The low temperature

experiments were taken directly out of the furnace in their holders, and tipped over into a large, deep, water-filled container.

2.4. Preparation of experiments for further investigation

The tube of a quenched experiment was broken open and the charge removed and split open to expose a cross-section. One half of the freshly exposed cross-section was mounted in epoxy under vacuum. The other half was kept as reference. Mounting under vacuum ensured that all air bubbles were removed from the epoxy, and that the epoxy filled all the pore spaces and cracks in the charge, so that a very good polish could ultimately be achieved. After polishing, each section was studied microscopically to ensure that representative areas of all the desired phases were visible. In binary systems no more than two phases can co-exist, and for this investigation all experiments were prepared to contain two phases in equilibrium. Sections were then photographed and prepared for analytical investigation. If one of the expected phases was not visible, grinding and polishing was continued. In some experiments, for example HU397, the PGE contents were very low, and the presence of a separate PGE alloy was suspected. This experiment was systematically polished away in 100 μm layers, but no alloy was found.

Total experimental charge weights varied from 0.25 gram to 2.0 gram, and more than one cross section was prepared from the larger experiments. In a number of experiments separated drops were found when the tubes were broken open. These drops, usually very small, could have separated before or during quenching. Drops formed during quenching would have equilibrated with the remainder of the experiment, and the composition would resemble that of the similar phases in the rest of the experiment. Drops formed before quenching probably did not equilibrate with the rest of the experiment. Each separated drop was investigated microscopically as well as analytically, to determine its relevance to each individual experiment.

Mounting and polishing difficulties were experienced due to hardness differences of co-existing phases. Metal is very malleable and co-exists in the different systems with sulphides such as digenite and pyrrhotite, both of which are very brittle. It was sometimes impossible to achieve a good polish of both the metal and the co-existing sulphide. Smearing of copper at very low concentrations was observed. This aspect is covered in a publication by Franklyn *et al.* (2001). In an investigation by Franklyn and Merkle (2001) tests were performed to determine the extend of smearing in various materials during polishing. Extensive smearing of PGE metals has also been reported by Makovicky *et al.* (1986) and Makovicky *et al.* (1990), but no discreet PGE phases were detected in this investigation, so that this possible complication could be ignored.

3. Microscopical Observations

3.1. Optical properties of quenched phases

3.1.1. Ni-S system

3.1.1.1. Nickel

White, very bright, isotropic (Figure 6).

3.1.1.2. Ni-S melt

Greenish cream, with exsolutions of nickel (Figure 6).

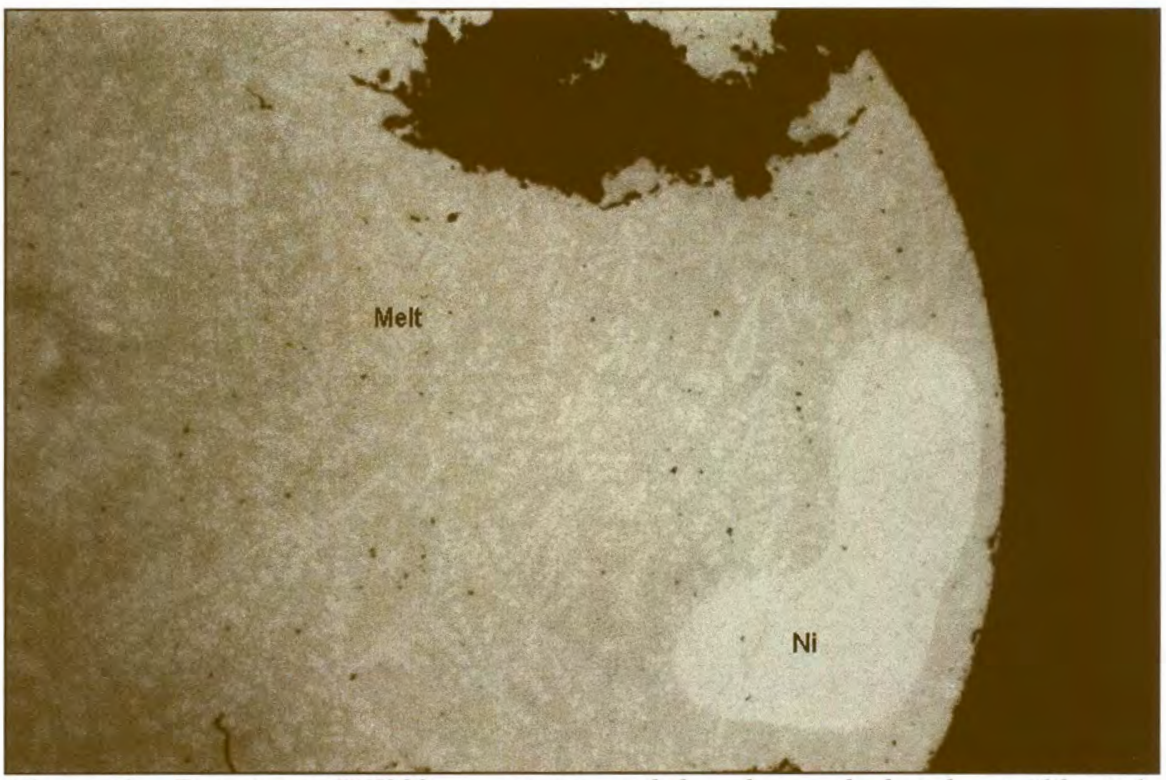

Figure 6. *Experiment HU393, co-existing nickel and quenched melt, equilibrated at 1000°C. Image was digitally enhanced. Field of view 4mm.*

3.1.2. Cu-S system

3.1.2.1. Copper

Bright, fresh pink, isotropic, tarnishes fast to reddish brown (Figure 7).

3.1.2.2. Digenite ($Cu_{2-x}S$)

Greyish blue, isotropic to weakly anisotropic. Twinning sometimes very pronounced, sometimes not visible. Shown in Figure 7 without twinning, and in Figure 8 with very clear twinning.

3.1.2.3. Cu-S melt

Three different melt compositions were investigated. The melt that co-exists with digenite has a similar colour (as well as similar composition) but is speckled with quench-phase alloys (Figure 8). The two immiscible melts investigated at 1200°C are similar in appearance to copper (the Cu-rich melt) and digenite (the S-rich melt), and are shown in Figure 9.

3.1.3. Fe-S system

3.1.3.1. Iron

Bright white, isotropic, tarnishes very quickly to grey-brown (Figure 10).

3.1.3.2. Troilite (FeS) and pyrrhotite (FeS_{1+x})

Both light yellow, strongly anisotropic, pyrrhotite weakly pleochroic (Figure 10, 26).

3.1.3.3. Fe-S melt

Creamy yellow colour, with quench-phase alloys visible, and sometimes a faint heterogeneous texture; anisotropic. Quench-phase alloy is visible in the melt shown in Figure 11.

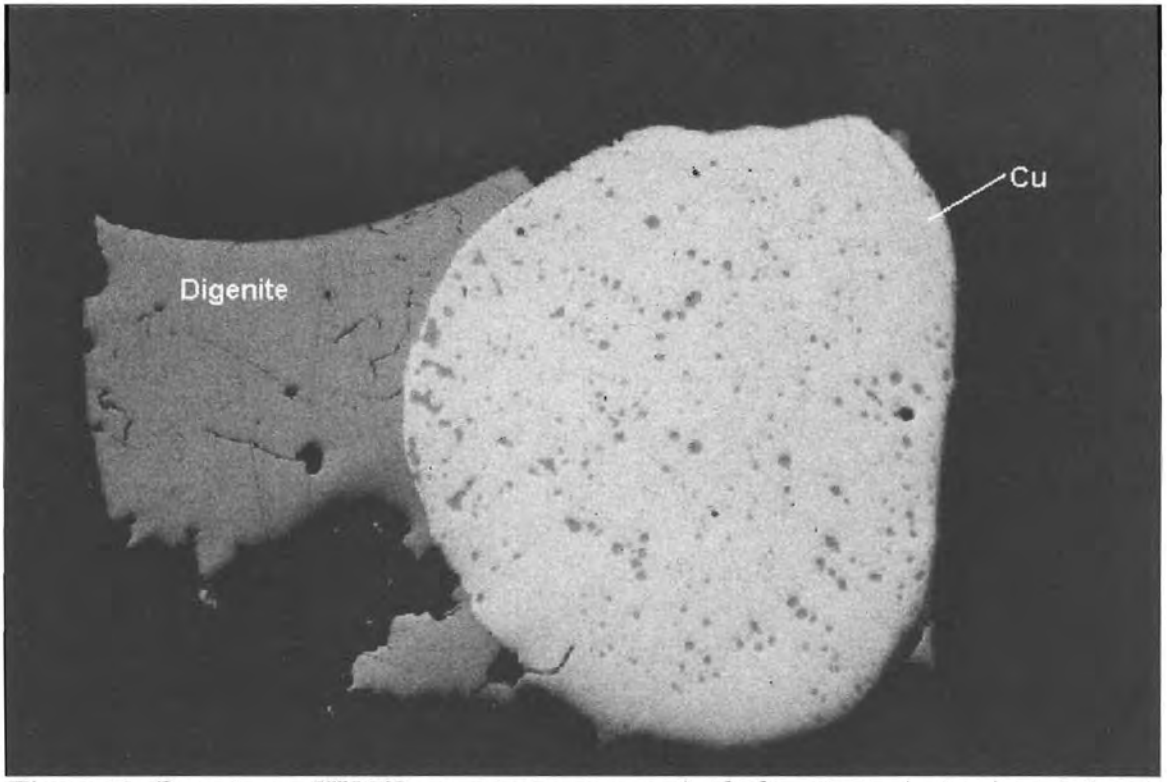

Figure 7. *Experiment HU465, co-existing copper (with digenite inclusions) and digenite, equilibrated at 1000°C. Field of view 4 mm long.*

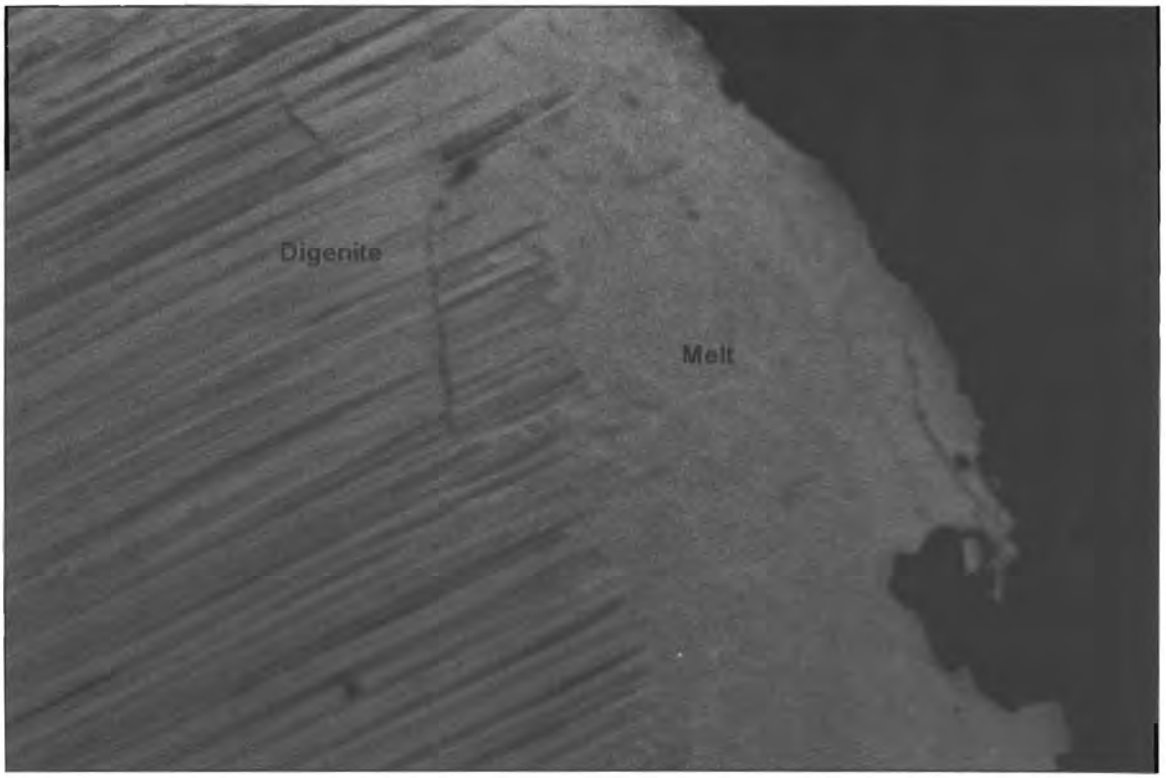

Figure 8. *Experiment HU420, co-existing digenite (twinned) and quenched melt, equilibrated at 1000°C. Image was digitally enhanced. Field of view2 mm.*

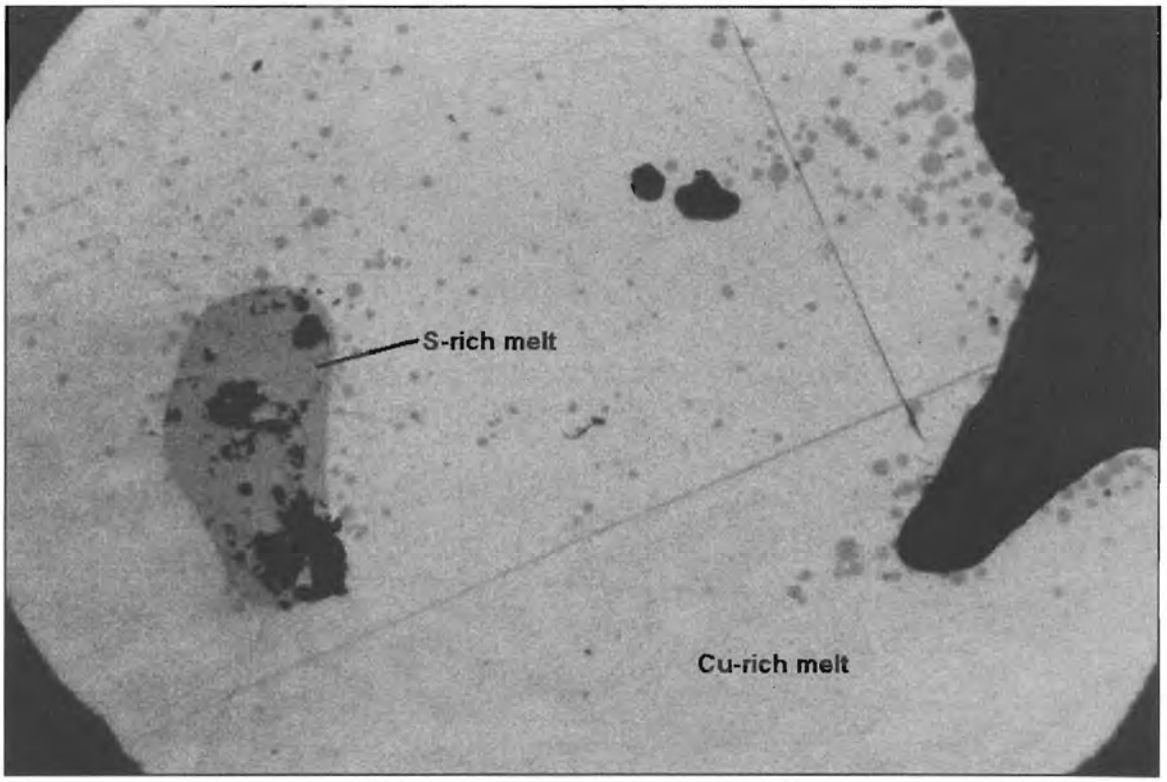

Figure 9. *Experiment HU442, co-existing immiscible Cu-rich melt and S-rich melt, equilibrated at 1200°C. Field of view 4 mm.*

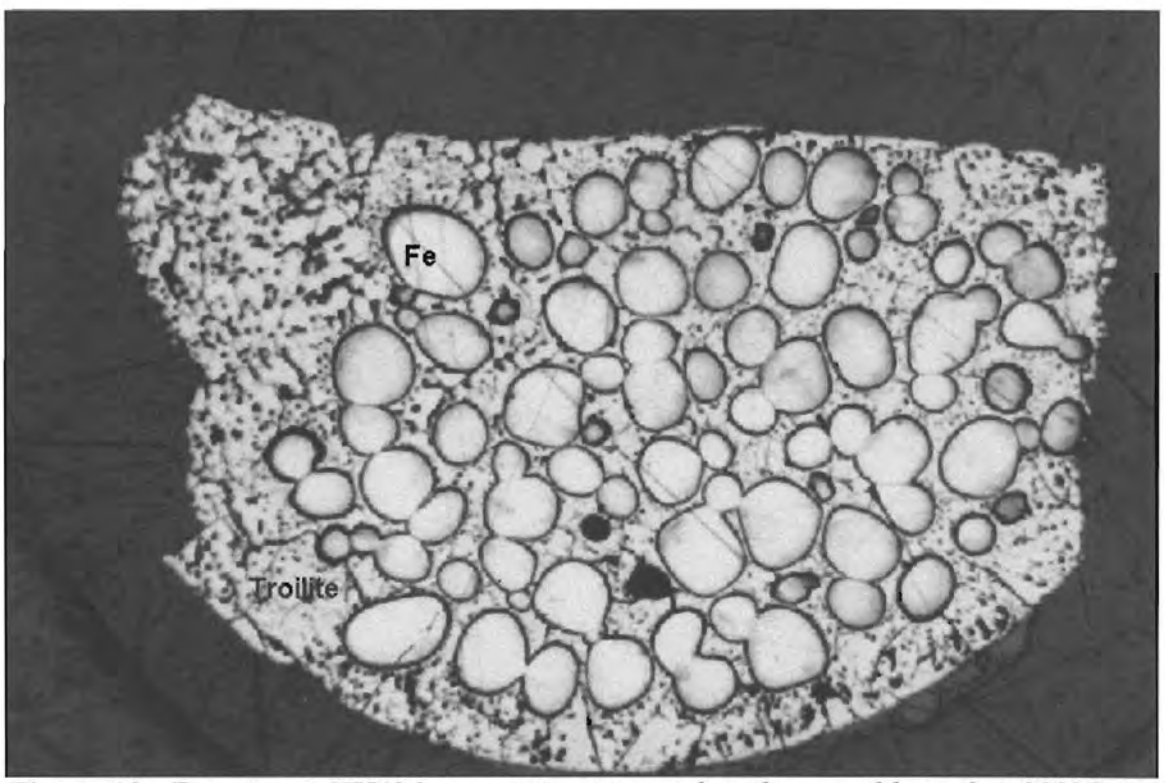

Figure 10. *Experiment HU436, co-existing iron and troilite, equilibrated at 900°C. Note the fast tarnishing of the iron to brownish colours. Field of view 4 mm.*

Figure 11. *Experiment HU736, Fe-S melt that co-exists with iron (not visible in this photograph), equilibrated at 1100°C. Image was digitally enhanced. Field of view 4 mm.*

3.2. Textures

3.2.1. Ni-S system

The phase diagram of the Ni-S system, after Sharma and Chang (1980) and Cemic and Kleppa (1986), is shown in Figure 12, where the initial bulk experiment compositions and expected equilibrated phase compositions in the present investigation are indicated. The assemblage investigated is described in Table 1.

3.2.1.1. Nickel - sulphide melt assemblage

The nickel globules mostly occur scattered evenly through the melt (Figure 13), but in some experiments they are concentrated in a specific sector of the melt (Figure 14), possibly as a result of gravity settling. Small bright specks of metal scattered through the heterogeneous sulphide melt (Figures 13 and 14) were formed during quenching, when the ability of the melt to contain Ni decreased during cooling. At equilibration temperature they were part of the melt phase, and were included during analyses of the melt. Fleet and Stone (1991) also reported quench-phase alloys, resulting from excess metal in their sulphide melt when it was quenched.

Table 1. *Assemblage of the Ni-S system that was investigated.*

Assemblage	Temp	Phase identification	Figures
Nickel - sulphide melt	1100 – 700°C	Nickel: bright white spherical globules. Sulphide melt: heterogeneous with quench-phase alloys.	13, 14

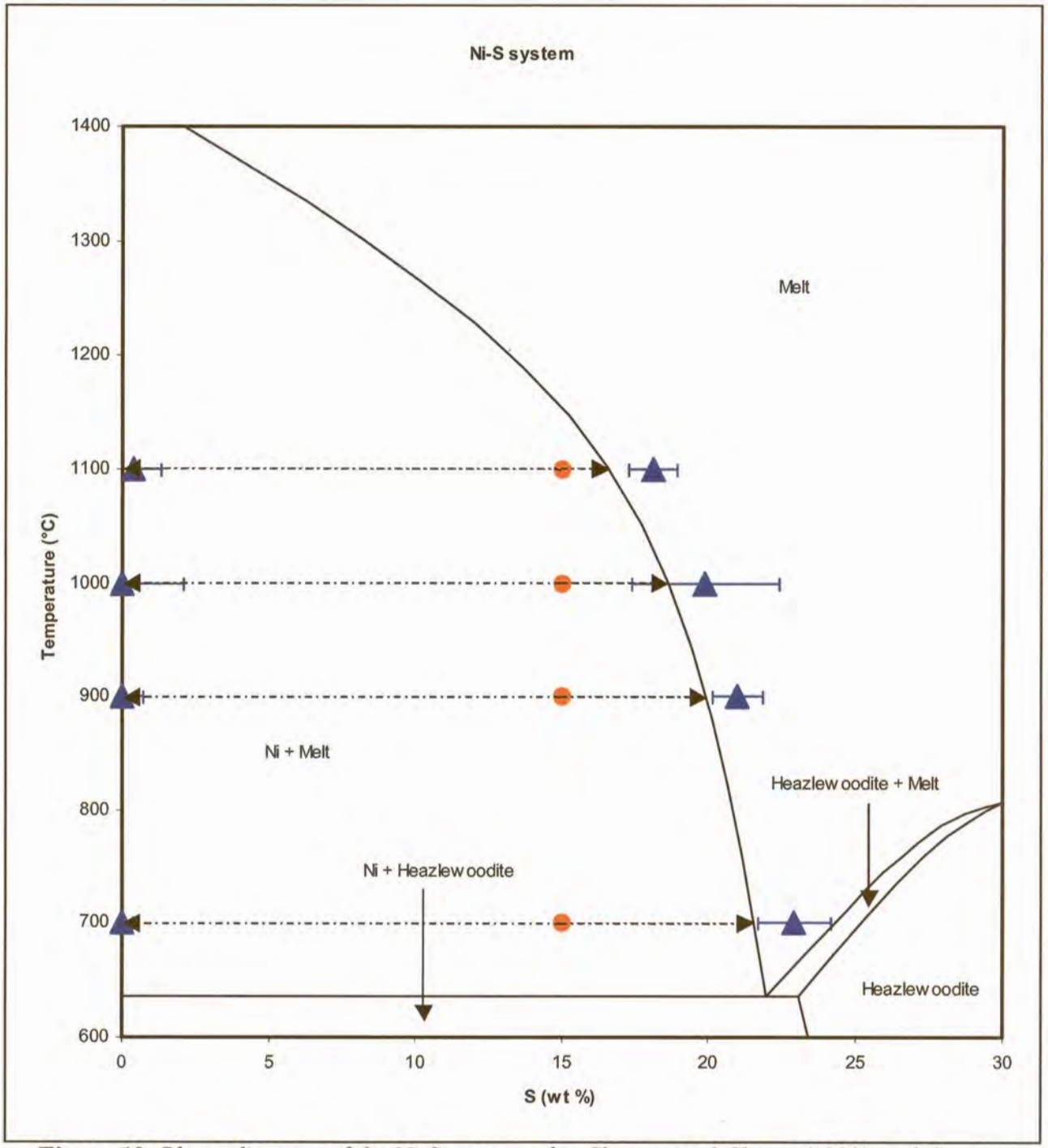

Figure 12. *Phase diagram of the Ni-S system, after Sharma and Chang (1980) and Cemic and Kleppa (1986). The red symbols indicate the bulk compositions of the experimental charges prepared to investigate the nickel - Ni-S melt assemblage, projected on the binary system. The expected compositions of the co-existing phases after equilibrium was achieved at the required temperatures are indicated by the tips of the arrows, and the average compositions of the equilibrated phases as determined by EPMA are indicated by the blue triangles, with error bars.*

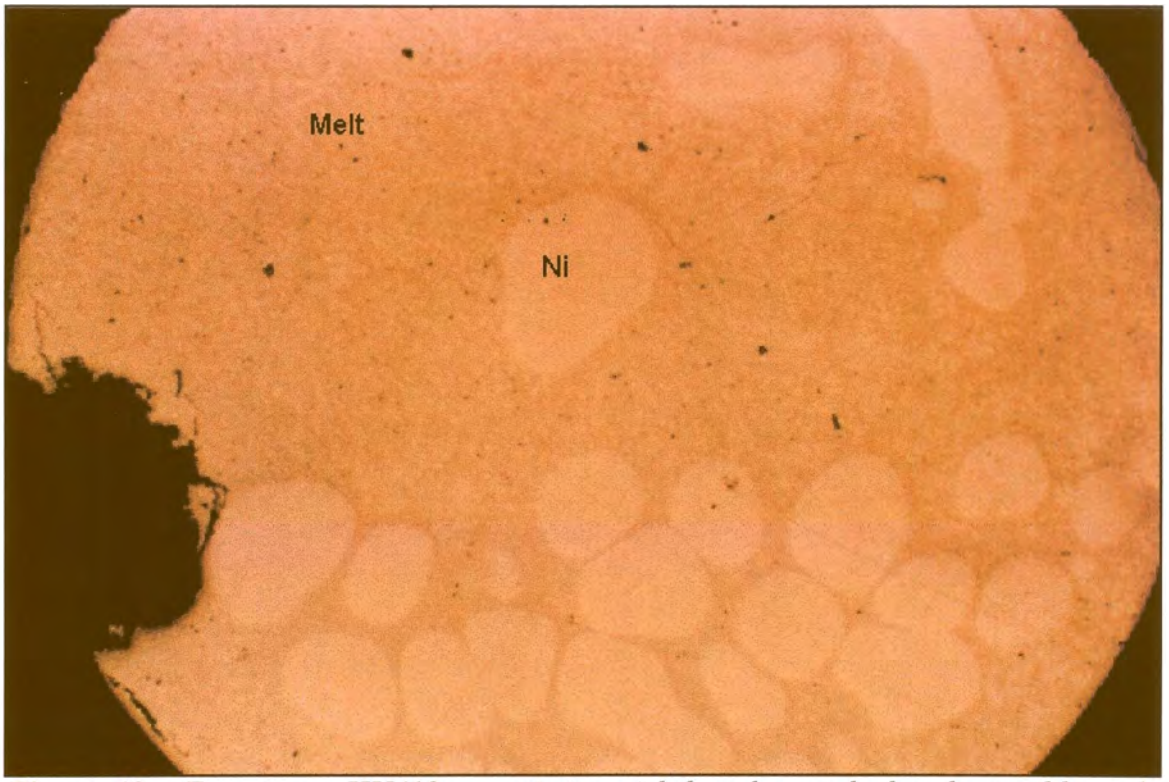

Figure 13. *Experiment HU412, co-existing nickel and quenched melt, equilibrated at 1000°C. Image was digitally enhanced. Field of view 4 mm.*

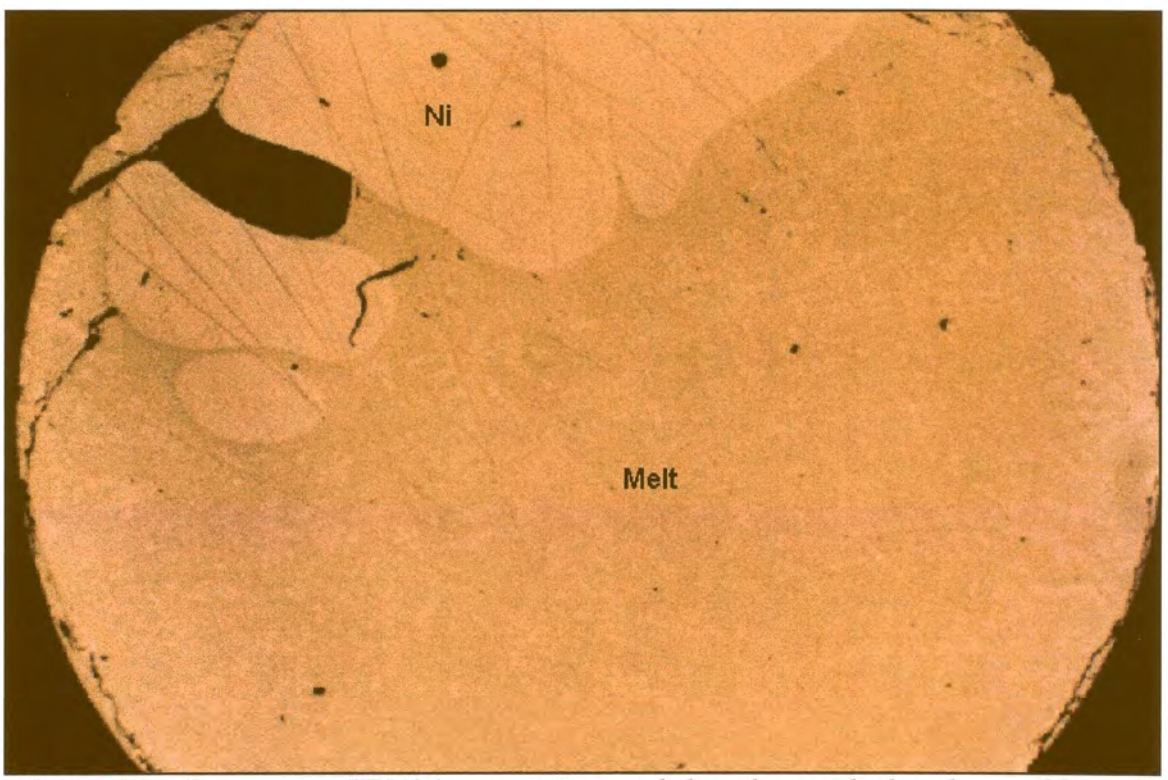

Figure 14. *Experiment HU426, co-existing nickel and quenched melt, equilibrated at 900°C. Image was digitally enhanced. Field of view 4 mm.*

3.2.2. Cu-S system

The phase diagram of the Cu-S system, after Chakrabarti and Laughlin (1986), is shown in Figures 15 and 16, where the initial bulk compositions and expected equilibration compositions of phases that were investigated are indicated. The assemblages that were investigated are discussed in Table 2.

Table 2. *Assemblages of the Cu-S system that were investigated.*

Assemblage	Temp	Phase identification	Figures
Copper - digenite	1000 – 700°C	Copper: viscous with high surface tension, commonly forms spherical drops in the centre of the experiments. Digenite: concentrated at the perimeter of the charge, forming a rim around the metal.	17, 18
Cu melt - digenite	1100°C	Cu melt: viscous, forms spherical drops in the centre of the experiments. Digenite: found along the perimeter of the experiment.	19, 20
Cu melt - sulphide melt	1200°C	Cu-rich melt: viscous, commonly forms spherical drops in the centre of the experiments, also scattered through sulphide melt as small spheres. Sulphide melt: mostly found along rim of experiment, but also dispersed as small and sometimes large spheres through Cu melt.	21, 22
Digenite - sulphide melt	1000°C	Digenite: occasionally shows clearly developed cleavage. Sulphide melt: slight heterogeneous appearance.	8, 23

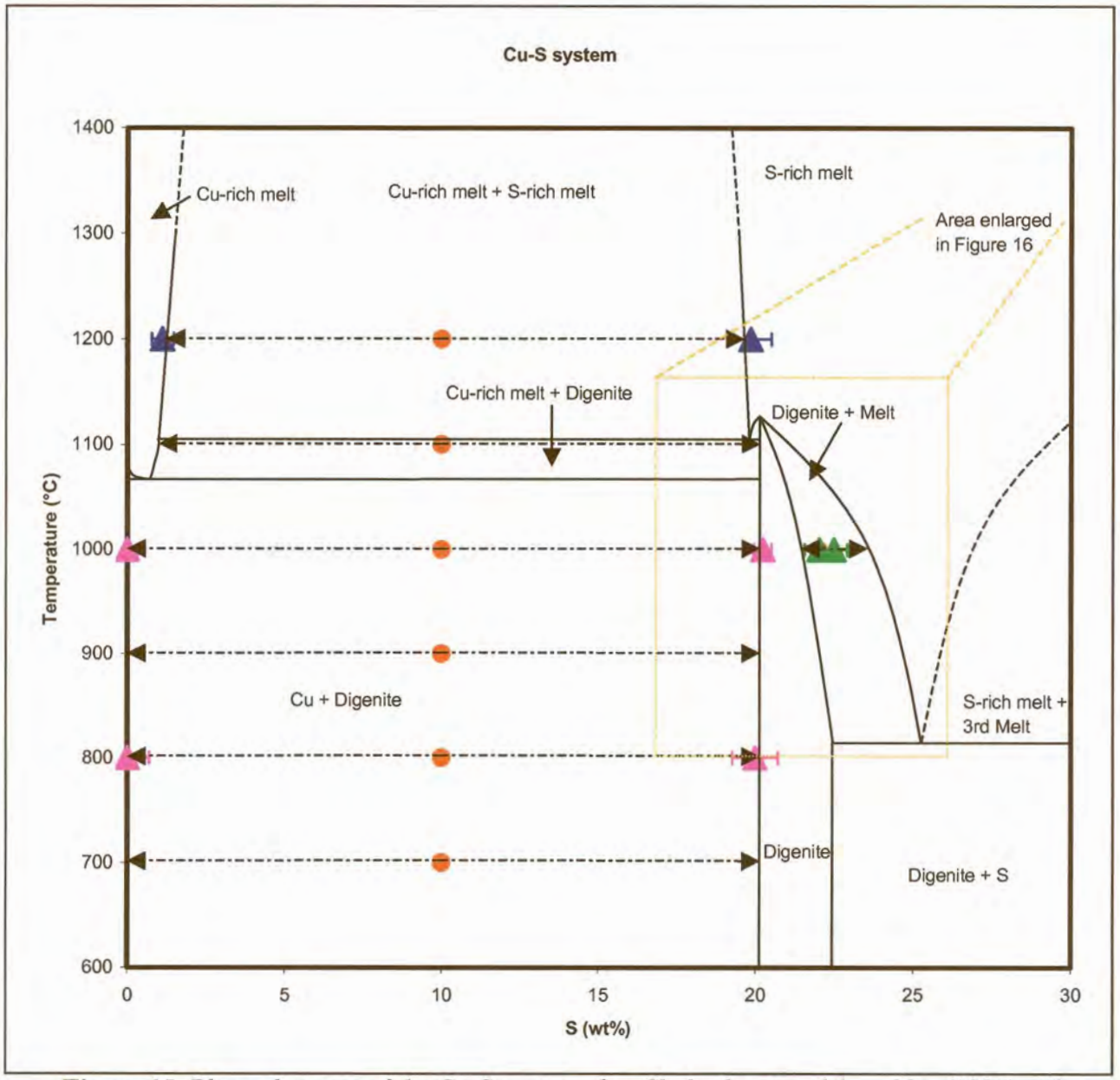

Figure 15. *Phase diagram of the Cu-S system after Chakrabarti and Laughlin (1986). The red symbols indicate the bulk compositions of the experimental charges prepared to investigate this system at various temperatures, projected on the binary Cu-S system, and the expected compositions of the resulting phases after equilibrium conditions were reached are indicated by the tips of the arrows. The blue triangles with error bars indicate the determined compositions of co-existing S-rich melt and Cu-rich melt at 1200°C, as determined by EPMA. The pink triangles indicate determined compositions of co-existing digenite and copper at 1000°C and 800°C, and the green triangles the determined compositions of co-existing digenite and melt at 1000°C. Experiments prepared to investigate co-existing Cu-rich melt and digenite at 1100°C and co-existing copper and digenite at 900°C and 700°C were too finely textured to analyse. These experiments will not be discussed further.*

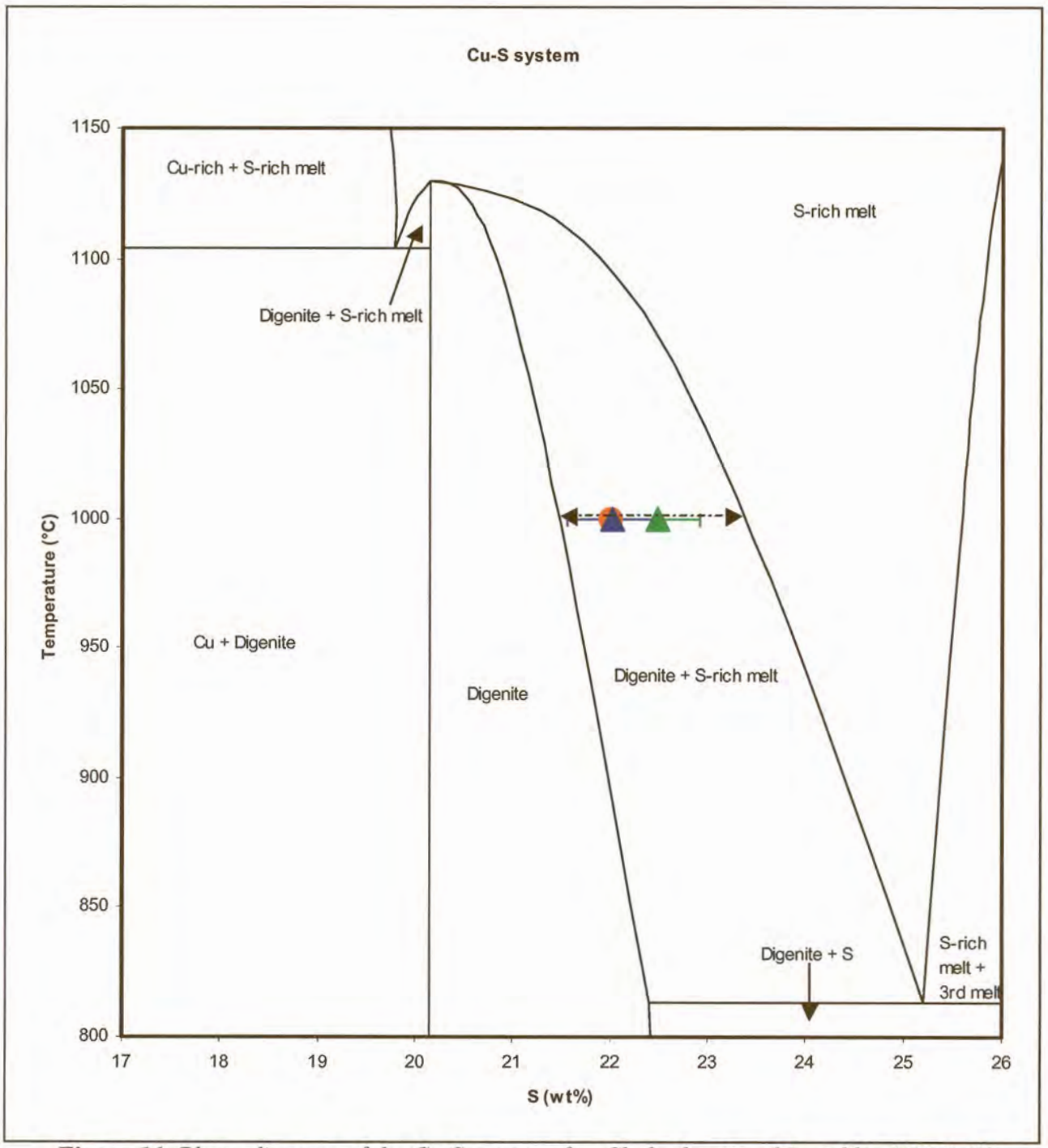

Figure 16. *Phase diagram of the Cu-S system after Chakrabarti and Laughlin (1986). The red symbols indicate the bulk compositions of the experimental charges prepared to investigate co-existing digenite and sulphide melt at 1000°C, projected on the binary Cu-S system, and the expected compositions of the resulting phases after equilibrium conditions were reached are indicated by the tips of the arrows. The blue triangle with error bars indicate the composition of the digenite, and the green triangle the composition of the melt, as determined by EPMA.*

3.2.2.1. Copper - digenite assemblage

The countless small drops of sulphide dispersed through the central copper core (Figure 18) could have formed on quenching, but they are less common in experiments that were equilibrated for longer periods. Despite leaving some experiments for long periods at high temperatures, small pieces of sulphide were still scattered through the copper. Experiment HU423 (Figure 18) was melted at 1100°C for 4 days, then equilibrated at 900°C for 51 days. Analyses of trace elements in the copper is complicated by the presence of these drops, as in-situ analytical methods also analyse in depth, where the presence of sulphides cannot be observed and avoided. If, however, the blebs are exsolutions that formed on quenching, their composition should be included with that of the metal. Practical difficulties were experienced during the mounting of these experiments. Because the sulphide is very porous and brittle, while the metal is malleable, the sulphide breaks away from the central copper core when the experiment is split open.

3.2.2.2. Cu melt - digenite assemblage

As in the copper - digenite assemblage (Section 3.2.2.1.), the sulphide crumbles away from the metal centre during mounting. Also, the Cu melt is speckled with sulphide (Figure 19), while the digenite is clear of Cu melt except for a few cracks (Figure 20). It was not possible to find areas of sufficient size clear of digenite for analysis of the melt, and this system was not analysed further.

3.2.2.3. Cu melt - sulphide melt assemblage

Of these two immiscible melts the Cu melt displays stronger surface tension, and generally forms a spherical blob in the centre of the charge surrounded by a rim of sulphide melt (see also Sections 3.2.2.1. and 3.2.2.2.). Both the Cu melt and the sulphide melt also occur as small droplets scattered throughout the other phase, in contrast to the previously discussed Cu-S assemblages (sections 3.2.2.1. and 3.2.2.2.) where only the sulphide melts show this behaviour.

3.2.2.4. Digenite - sulphide melt assemblage

The chemical compositions of the digenite and the sulphide melt and their optical characteristics are very similar. In some instances, the digenite is clearly twinned (Figure 8), but otherwise the only way to distinguish between the two phases is by the heterogeneous appearance of the melt (Figure 23).

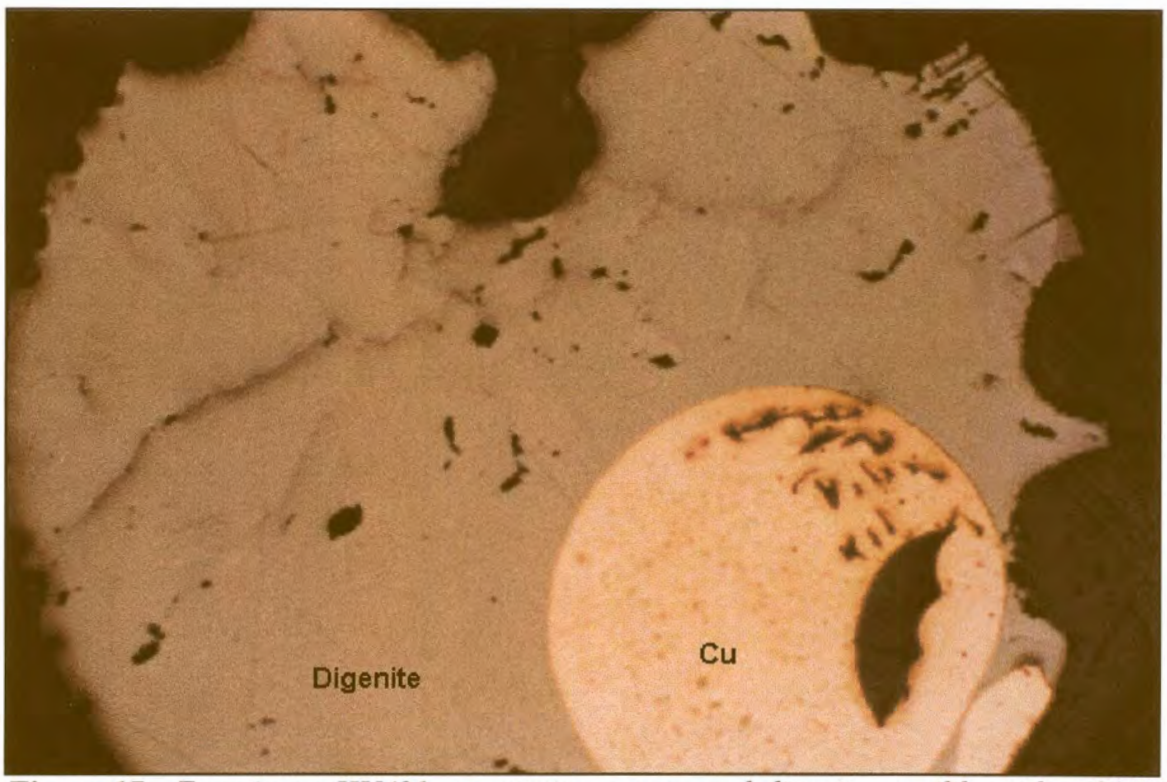

Figure 17. *Experiment HU421, co-existing copper and digenite, equilibrated at 900°C. Sulphide blebs scattered through the metal vary in size from extremely small to large. Field of view 4 mm.*

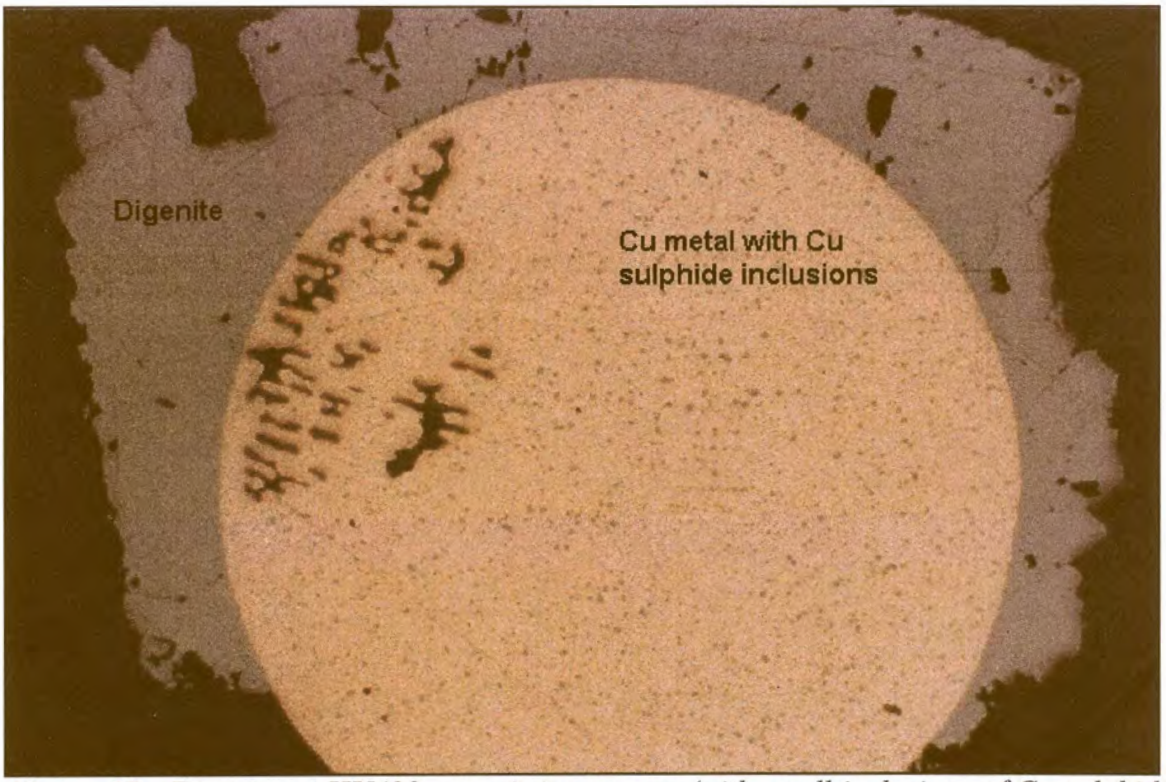

Figure 18. *Experiment HU423, co-existing copper (with small inclusions of Cu sulphide) and digenite, equilibrated at 900°C. Field of view 4 mm.*

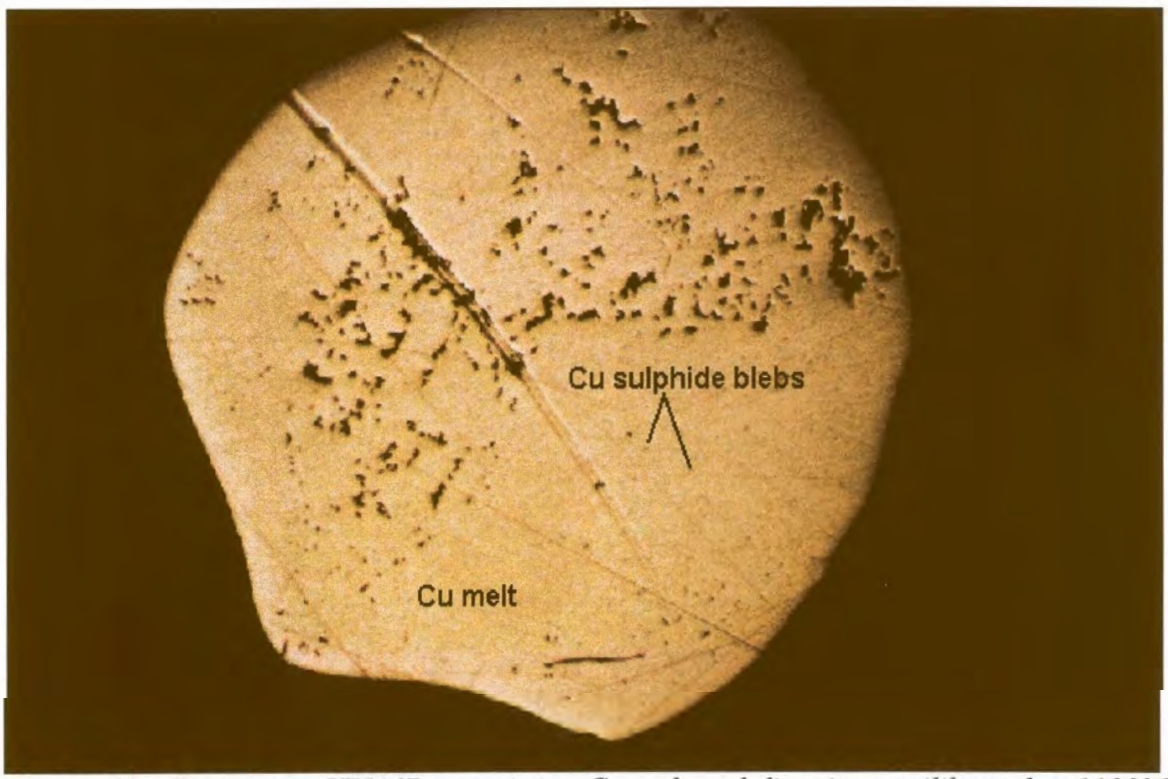

Figure 19. *Experiment HU467, co-existing Cu melt and digenite, equilibrated at 1100°C. The Cu melt contains small sulphide blebs. Image was digitally enhanced. Field of view 4 mm.*

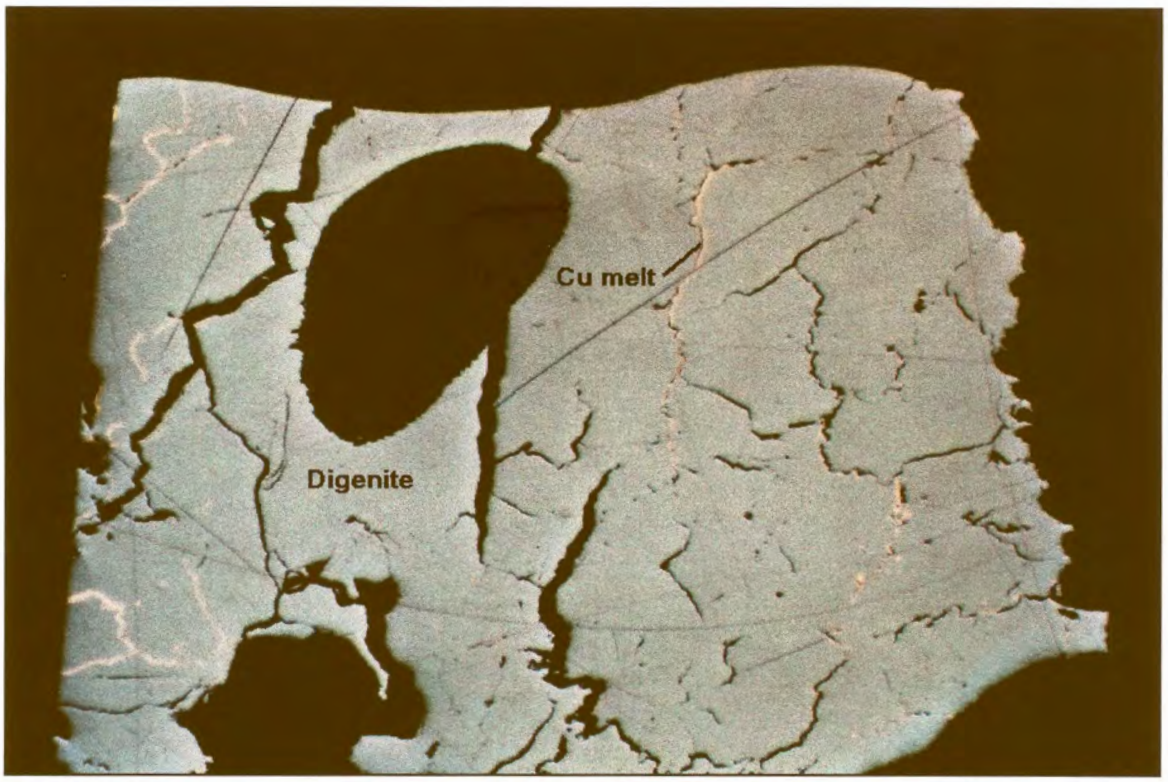

Figure 20. *Experiment HU467, digenite with quenched Cu melt filling the cracks, equilibrated at 1100°C. Image was digitally enhanced. Field of view 4 mm.*

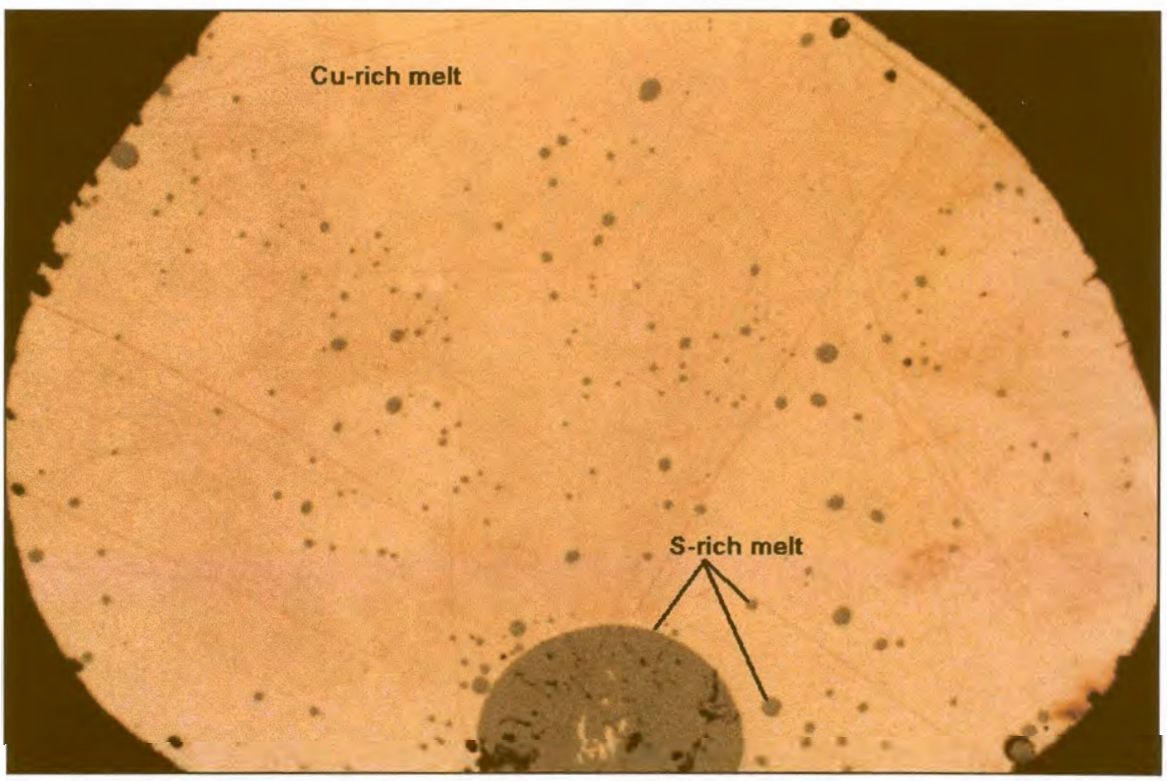

Figure 21. *Experiment HU445, co-existing immiscible Cu-rich and S-rich melts, equilibrated at 1200°C. The sulphide melt rim broke away from this central section during mounting, but sulphide melt is also observed as small and larger spheres dispersed through the Cu melt. Field of view 4 mm.*

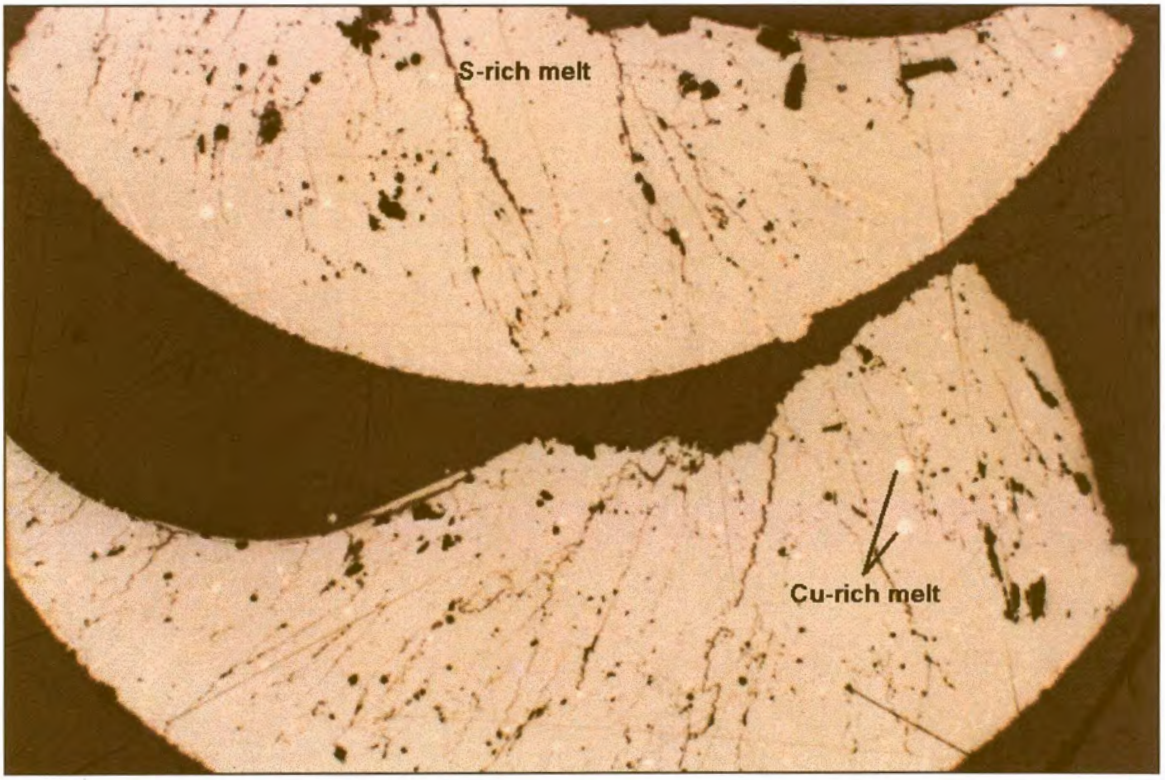

Figure 22. *Experiment HU445, equilibrated at 1200°C. S-rich melts as found around the rim of the experiment shown in Photograph 21, with Cu-rich melt present as small spheres scattered through the sulphide melt. Image was digitally enhanced. Field of view 4 mm.*

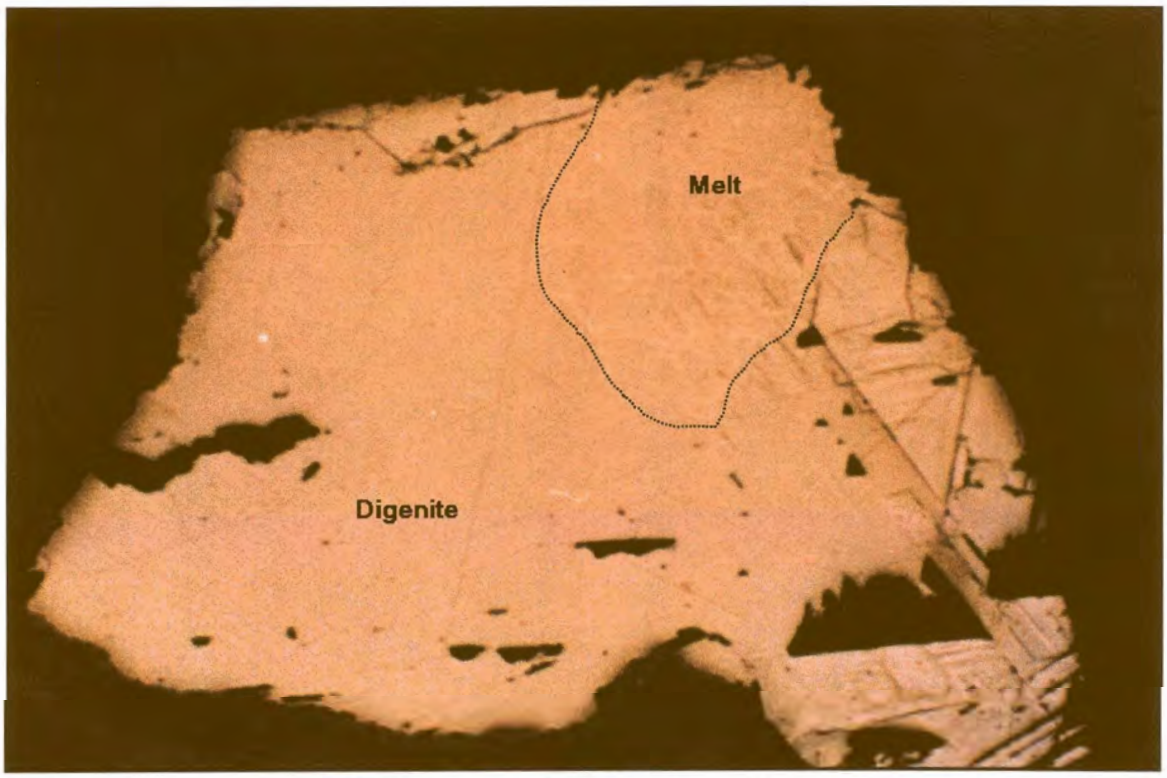

Figure 23. *Experiment HU418, co-existing digenite and quenched melt, equilibrated at 1000°C. Without visible twinning of the digenite, the melt phase can be identified by its heterogeneous appearance. Image was digitally enhanced. Field of view 4 mm.*

3.2.3. Fe-S system

The phase diagram of the Fe-S system, after Chuang *et al.* (1985), is shown in Figure 24, indicating the investigated assemblages which are described in Table 3.

***Table 3**. Assemblages of the Fe-S system that were investigated.*

Assemblage	Temp	Phase identification	Figures
Iron - sulphide melt	1200 – 1000°C	Iron: bright white with good polish. Sulphide melt: creamy yellow, lower reflectivity and hardness than metal.	25
Pyrrhotite - sulphide melt	1100°C	Both phases have a creamy yellow colour, similar reflectivity and hardness.	26
Iron - troilite	900°C	Iron: bright white with good polish. Troilite: dull yellow, very brittle with bad polish.	10, 27

3.2.3.1. Iron - sulphide melt assemblage

The iron occurs as roundish blebs dispersed through the sulphide melt matrix. Occasionally small exsolutions of iron, which form skeletal textures, occur scattered through the melt. These small pieces of metal were produced during quenching, and formed part of the melt at the equilibration temperatures.

3.2.3.2. Pyrrhotite - sulphide melt assemblage

There is not a clear optical distinction between the melt and the pyrrhotite, possibly due to the similarity in the compositions (phase diagram - Figure 24). The phases are intergrown with curving boundaries, but the melt is slightly heterogeneous with darker and lighter zones, which makes identification possible.

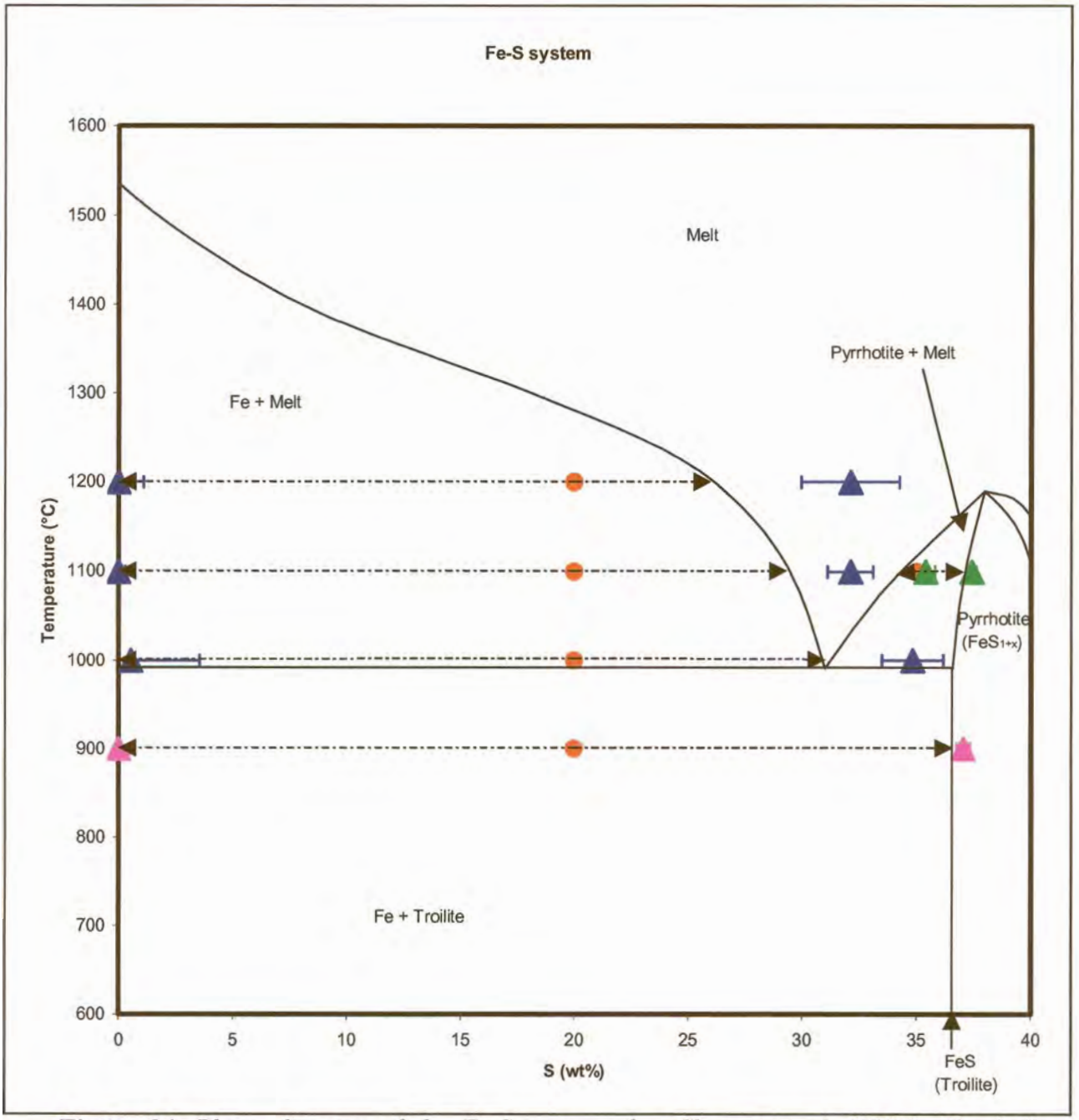

Figure 24. *Phase diagram of the Fe-S system after Chuang et al. (1985). The bulk compositions of the experimental charges are indicated by the red symbols, the expected compositions of the co-existing phases after equilibrium was reached by the tips of the arrows, and the true compositions of the co-existing phases as determined by EPMA are projected onto the diagram and indicated by the triangles. The blue triangles with error bars indicate the F:S ratio of co-existing iron and sulphide melt, the pink triangles the Fe:S ratio of co-existing iron and troilite, and the green triangles the Fe:S ratio of co-existing pyrrhotite and sulphide melt. Many of these experiments were oxidised.*

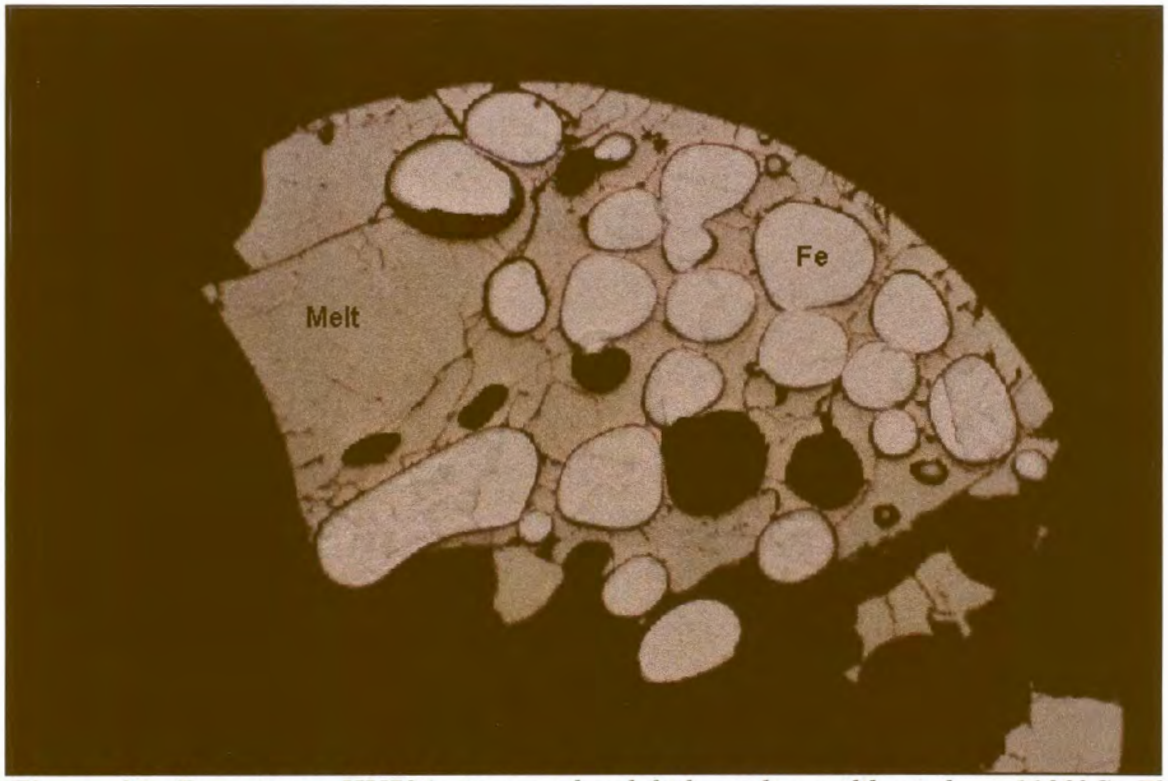

Figure 25. *Experiment HU734, iron and sulphide melt equilibrated at 1100°C. The sulphide melt appears homogeneous on this scale. Field of view 4 mm.*

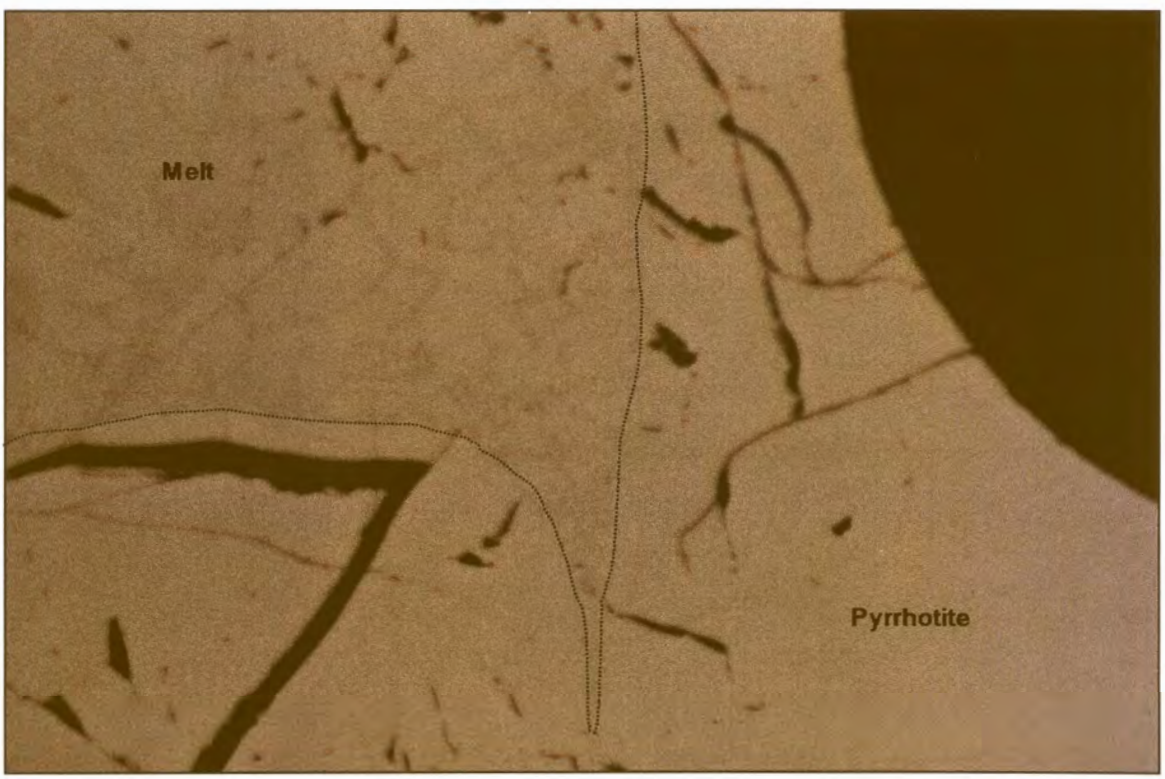

Figure 26. *Experiment HU739, co-existing pyrrhotite and quenched sulphide melt equilibrated at 1100°. The melt can be distinguished from the sulphide only by its heterogeneous appearance. Image was digitally enhanced. Field of view 1.4 mm.*

3.2.3.3. Iron - troilite assemblage

The iron occurs as round blebs scattered through the troilite, which forms the matrix.

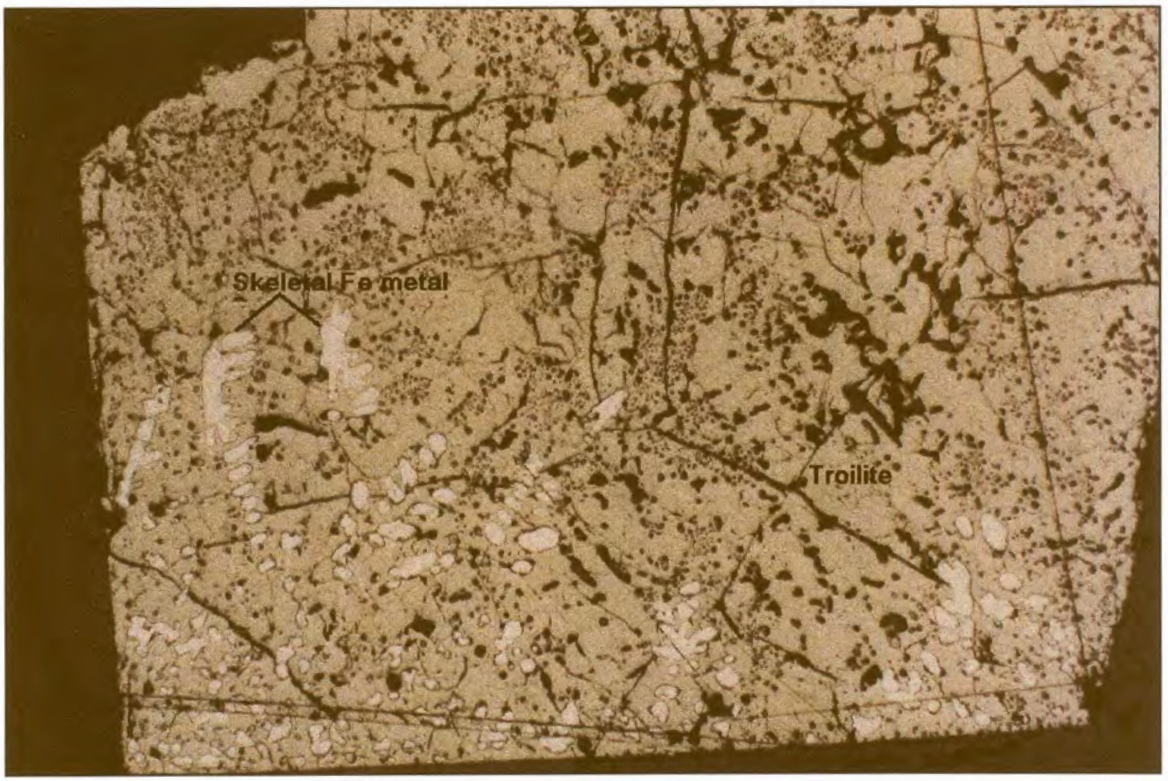

Figure 27. *Experiment HU436, containing troilite and dendritic iron, equilibrated at 900°C. Field of view 4 mm.*

4. Analytical Techniques

4.1. Electron Probe Micro Analysis (EPMA)

Areas of interest for microprobe analysis were selected by microscopic investigation. Reflected light photographs of these areas were used for reference and orientation during microprobe analysis. Polished sections were coated with a 20 to 25 nm conductive carbon layer.

A JEOL 733 Superprobe was used to analyse for the major element contents at an accelerating voltage of 20 KeV and a beam current of 20 nA, measured on a Faraday cup, in wavelength-dispersive (WD) mode. Counting times were 50 seconds on the peak and 25 seconds on the backgrounds. For the metals, pure Cu, Ni and Fe were used as standards. For the sulphides, millerite was used as a standard for nickel sulphides and chalcopyrite for copper and iron sulphides. Spot analyses, with a diameter of <2 μm, were made of the metals and sulphides. Standards were routinely measured before, during and after analysis to control instrumental drift.

To analyse the heterogeneously quenched Cu-S, Ni-S and Fe-S melts, representative areas of the melts were analysed in scanning mode. The sizes of the analysed areas were selected according to the size of the quench-phase alloys in the solidified melts as well as the areas of melt available between the crystals of the primary solid phase, but were generally about 200 μm^2. The heterogeneity of the quenched melt was compensated for in this way. For the Ni-S and Cu-S melts, two types of standards were tested: synthetically prepared quenched melt phases as well as the sulphides described above. No difference was found in the quality of the analyses. Heterogeneous textures containing quench-phase alloys have also been analysed by other authors (e.g. Fleet and Stone, 1991), who applied a defocussed electron beam to obtain bulk chemical analyses of quenched liquids. This method was also tested in the present investigation, but resulted in very large standard deviations, and the technique of scanning the beam over an area on the sample is preferred. The standard

deviations of quenched melt analyses reflect true compositional differences. If a very large number of 1 μm beam spots was used to analyse the same phase, it would result in similar element averages as the result of a few large area scans, but the standard deviations would be much larger. All EPMA results of quenched melts provided in this report were performed with area scans, except when specified otherwise.

Occasional EPMA analyses of PGE contents were performed with pure Rh, Pd and Pt as standards for the PGE, Cu-, Ni- and Fe sulphides for the melts and sulphides, and Cu, Ni and Fe for the metals.

The results of analyses of the Ni-S melt phases described in Section 5.1.1.1. were found to be consistently more S-rich than predicted by the phase diagram of the Ni-S system (Sharma and Chang, 1980) at all four temperatures investigated. Duplicate analyses were performed to confirm the quality of the results. Area scans of 200 μm^2, 40 μm diameter spot analyses as well as 600 1μm diameter spot analyses all resulted in similar average melt compositions, enriched in S compared to the phase diagram. Different sulphide standards were used with no difference in results. The analyses are consistent, and no analytical explanation for the deviation from the published phase diagram can be given.

Detection limits for PGE in metals and sulphides are 200 to 300 ppm with the EPMA, which is not sufficient to determine the low PGE contents of interest in this investigation. An additional analytical technique (PIXE) had to be considered, as discussed in the following section. Only the major elements (Ni, Cu, Fe and S) were routinely determined by EPMA. Trace PGE were ignored during EPMA analyses of major elements, as their effect on the correction factors would be smaller than the analytical uncertainty due to counting statistics.

4.2. Particle Induced X-ray Emission (PIXE) Analysis

PIXE is a non-destructive, in-situ multi-element analytical technique, capable of detection limits down to the ppm level (Halden *et al.*, 1995). The sample is bombarded with high

energy protons (or other particles) to generate characteristic X-rays from the sample. These protons are less easily scattered than electrons (Johansson, 1992). Czamanske *et al.* (1993) reported that the X-rays emitted by the sample after MeV energy proton bombardment to be quantitatively similar to those emitted by KeV energy electron bombardment. However, the bremsstrahlung background is much lower with PIXE, so that the ratio of characteristic X-rays to background is much higher (Cabri *et al.*, 1984a; Remond *et al.*, 1987; Sie *et al.*, 1989a; Johansson, 1992), which lowers detection limits considerably. The secondary bremsstrahlung emitted by electrons set in motion by the primary protons determines the limit of detection (Halden *et al.*, 1995). A focused beam of protons, or other particles, with a spot size of a few square microns or more can be used for point analysis, or the beam can be scanned over larger areas to provide a two-dimensional X-ray map of element distribution (Halden *et al.*, 1995). Cabri (1988) and Sie *et al.* (1989a) expanded on the practical aspects of combining EPMA and PIXE analysis applied to geological and mineralogical investigations. Both techniques use focused beams of charged particles to excite characteristic X-rays. EPMA can be utilised for major element determinations while PIXE is very successful for determining trace element concentrations, especially in simple matrixes (Campbell *et al.*, 1990), as demonstrated by Remond *et al.* (1987) on determination of trace concentrations of In, Se and Hg, undetectable with EPMA, with micro-PIXE.

Minimum detection limits of 1.2 to 3 ppm for Pd and Rh, and 50 to 60 ppm for Pt in sulphides were obtained by Cabri *et al.* (1984b). Cousens *et al.* (1989) and Paktunc *et al.* (1990) used the technique to investigate partitioning of PGE and other trace elements in sulphides from the Bushveld Complex. PIXE analyses for many elements, including PGE, were performed by Czamanske *et al.* (1992) on sulphide ores from the Norilsk-Talnakh district. Milli-PIXE analysis of platinum-group minerals from the Witwatersrand basin was employed by Merkle and Franklyn (1999) to determine trace element contents in an attempt to obtain information on the sources of the grains. Sie *et al.* (1989b) used PIXE in combination with fire-assay to determine PGE and Au at sub-ppm levels suitable for application in exploration.

There are some contradictions regarding analysis depth and surface effect of EPMA compared to PIXE. According to Campbell *et al.* (1990) a significant difference between EPMA and micro-PIXE is that the depth analysed with micro-PIXE is about 10 times greater. Remond *et al.* (1987) verified by calculation of X-ray yields that the accuracy of micro-PIXE measurements are less influenced by surface contamination than for EPMA. This statement is directly contradicted by Franklyn and Merkle (1999), but still requires quantification. Ryan *et al.* (1990) calculated that a typical PIXE beam spot of 20µm diameter at 10 nA excites X-rays from depths often greater than 40µm in the matrix. Variation of excitation depth for different elements in different matrixes, varying from Zr X-ray yields from a depth of 39.7 µm in a matrix with density 2.7 (feldspar), to an excitation depth as low as 10.1 µm for Ni in a matrix with density 5.5 (chromite), was reported by Cabri and Campbell (1998). The area analysed by EPMA is usually a few μm^2, while the area analysed by micro-PIXE is sometimes much larger. This problem was pointed out by Franklyn and Merkle (1999), who compared 1 µm diameter EPMA point analysis results with 100 µm diameter milli-PIXE analyses. It was more difficult to ensure that only one phase was analysed with a larger milli-PIXE beam spot. The penetration depth of the proton beam also has to be considered when choosing a position for analysis, and homogeneity at depth in a sample has to be established, as X-rays may be excited from beneath the phase under investigation (Halden *et al.*, 1995). The relatively large effective area of analysis of PIXE results in better averaging of the sample - larger beams obtain a better averaging effect (Sie *et al.*, 1989b; Franklyn and Merkle, 1999). Remond *et al.* (1987) reported that contamination or surface changes can be introduced during mechanical polishing or during electron or proton beam irradiation.

4.2.1. Milli-PIXE

The analyses were performed on the same PIXE beam line with the same set-up described by Franklyn and Merkle (1999). Quadrupole magnets are used to focus the 3 MeV H^+ beam from the Van De Graaff Accelerator to a 2 mm diameter beam spot, which is then collimated to 100 µm diameter with two 100 µm carbon collimators. The collimators are spaced 200 mm apart, with the last collimator 120 mm from the target position. The term

milli-PIXE is appropriate to describe this system with a beam diameter of 100 µm. X-rays emitted from a 50 µm thick W wire that was moved across the beam were used to determine the spatial distribution of the beam. A halo contribution of less than 0.5 % was observed at 0.2 mm from the beam centre. Beam currents of up to 1 nA were used on the targets. The polished epoxy mounts containing the samples were initially oriented at a 45° angle to the incoming beam, with the detector at 45° to the sample surface. This meant that the impact area on the sample surface was oval and the longest elongation greater than 100 µm (see Photograph 20). During later analyses, the samples were mounted perpendicular to the incoming beam, with the detector at a 45° angle to the sample. Energy-dispersive X-ray analysis was performed utilising a germanium detector, with FWHM resolution of 165 eV at 5.9 KeV, initially mounted at 90° to the beam direction, but later changed to 45°. The detector had a 25 µm thick Be window and the exit window of the PIXE chamber consisted of 23 µm of Mylar. Pile-up suppression in the X-ray spectra was obtained through dynamic beam pulsing, and electronic pile-up rejection was used to reduce doubling (Franklyn and Merkle, 1999).

The spectra were processed with the GUPIX software package developed at Guelph for PIXE analysis (Maxwell *et al.*, 1989, 1994, 1995). GUPIX was used by Campbell *et al.* (1996) in the analysis of silicate reference standards, and was also evaluated by Czamanske *et al.* (1993). A model spectrum containing all relevant X-ray lines is fitted to the measured spectrum by non-linear least squares, the background continuum being removed by digital filtering (Maxwell *et al.*, 1989). Relative intensities of element lines are adjusted to reflect matrix effects, absorber transmission and detector efficiency. The elemental concentrations for PIXE are obtained by reference to a single element in the same spectrum that can be analysed independently (Rogers *et al.*, 1987), and in the present investigation this was achieved by the EPMA analyses of major elements. According to Rogers *et al.* (1987), the disadvantage of internal normalisation, where relative intensities are calculated from theory and compilations of experimental data, is that the errors in the final values are difficult to determine. Calculation of the final uncertainty is further complicated by spectrum fitting errors and uncertainties in the filter absorption and the amplifier calibration. Fitting errors are believed to predominate over errors in relative intensity calculations.

Detection limits decrease in inverse proportion to the square root of the measurement duration (Czamanske *et al.*, 1993) or, as stated by Halden *et al.* (1995), detection limits depend on the total charge used during analysis and therefore on the total accumulated counts, which is increased by longer counting times. This implies that lower detection limits can be obtained by increasing analysis time. For each spectrum the principal peak for each element is evaluated with a 3σ standard deviation, which reflects both counting statistics and error from peak overlap, and a lower limit of detection. In the present investigation, the detection limit for each PGE, together with the error or standard deviation, is given for every individual analysis, but the lowest detection limits obtained in each analysed phase are summarised in Table 4. Traditionally EPMA analyses are described by, amongst other factors, the analysis time on the peaks and background. However, the milli-PIXE analyses were performed by considering the total number of counts detected during each analysis. These counts are provided along with the other information for each milli-PIXE analysis in this investigation.

Table 4. *Detection limits obtained for the PGE by milli-PIXE.*

Phase	Rh LLD (wt%)	Pd LLD (wt%)	Pt LLD (wt%)
Nickel	0.009	0.004	0.011
Ni-S-melt	0.013	0.014	0.020
Cu-rich melt	0.016	0.013	0.031
S-rich melt	0.011	0.014	0.031
Copper	0.025	0.021	0.024
Digenite	0.013	0.014	0.036
Iron	0.020	0.040	0.040
Fe-S-melt	0.020	0.030	0.030
Pyrrhotite	0.030	0.020	0.040
Troilite	0.040	0.040	0.050

The S-rich melt of experiment HU443 was analysed seven times, but it was suspected that one of these measurements was influenced by another phase and was ignored. In each of the six remaining analyses, shown in Table 5, the Pt content was below the detection limit. The

fourth analysis was left to collect 400000 counts - more than any of the other analyses - and the detection limit that was obtained was the lowest of all the analyses. In Figure 28 the detection limits obtained for each of the analyses are plotted against the number of counts collected, showing that increased count collection lowers the detection limit. The scatter in the points indicates that the detection limit is not only a function of the total counts collected. Other factors, such as the precise alignment of all the components in the PIXE line, and the fine-tuning of the electronics, both of which are dependent on temperature and pressure which change during long work sessions, also influence the LLD's. The GUPIX program does not have the option of combining results to obtain very low detection limits.

***Table 5**. Repeated measurement of the S-rich melt of experiment HU443, showing a relationship between total counts collected and detection limit.*

Exp	Pt wt% (± 3σ)	Pt LLD	Counts
HU443	*0.003* (0.026)	0.048	200000
HU443	bd	0.057	200000
HU443	*0.015* (0.018)	0.031	400000
HU443	*0.036* (0.032)	0.053	100000
HU443	*0.024* (0.030)	0.053	100000
HU443	*0.007* (0.037)	0.067	100000

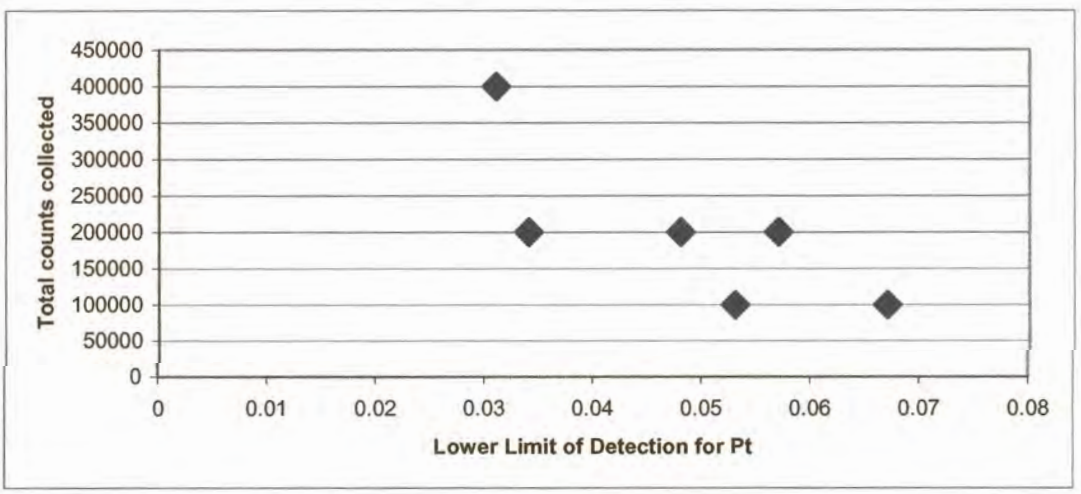

***Figure 28.** The influence of counts collected on the detection limit of Pt in the S-rich melt of experiment HU443.*

When an element could not be detected, it was assumed that the concentration of that element was lower than, or equal to, the detection limit, and the detection limit was used as the maximum content of that element for further calculations.

An advantage of PIXE is its independence of matrix matched external standards (Ryan *et al.*, 1990). The problem of non-availability of trace element standards, as well as the problem of heterogeneity of trace element standards on the micron scale, are eliminated. Standards of pure Rh, Pd and Pt as well as Cu, Ni and Fe were used to determine and correct for peak shift.

Similar to EPMA analyses, a thin conductive carbon coating on the sample surface is required for analysis. Areas to be analysed were identified prior to insertion of the sample into the PIXE chamber. No optical system was available to orient the sample once it was sealed inside the vacuum chamber, and positions were determined by monitoring X-ray spectra while moving the sample through the beam to determine its shape and precise orientation, and with the assistance of reflected light photographs of the grains, the required positions for analyses were determined. As far as possible, the same areas analysed by EPMA were analysed by PIXE.

4.2.1.1. Evaluation of analytical conditions

As the major element contents (Cu, Fe, Ni, S) in the experiments are much higher than the PGE contents, the X-rays from these elements are very pronounced, and together with the resulting background, normally overlap completely with the PGE peaks. Due to the presence of more than 20 wt% S in half of the analyses, an Al filter had to be used to absorb most of the low energy S X-rays. The use of thick filters in micro-PIXE has a major effect on the low energy portion of the ED spectrum. Remond *et al.* (1987) used a 750 µm thick Al filter, which made detection of Cu and Fe, known to be present in their samples, impossible. For the results reported here, experimentation with different filter thickness and even beam acceleration voltage was necessary to obtain the best possible conditions for PGE detection.

A spectrum acquired at 2.45 MeV on the Ni-S melt phase in experiment HU429 (Figure 29), which contains about 20 wt% S, 80 wt% Ni and traces of Pt, Pd and Rh, is shown in Figure 30. The white specks in Figure 30 indicate the number of counts detected in every energy channel, from low energy (left) to high energy (right) radiation, to form an X-ray spectrum of the analysed spot.

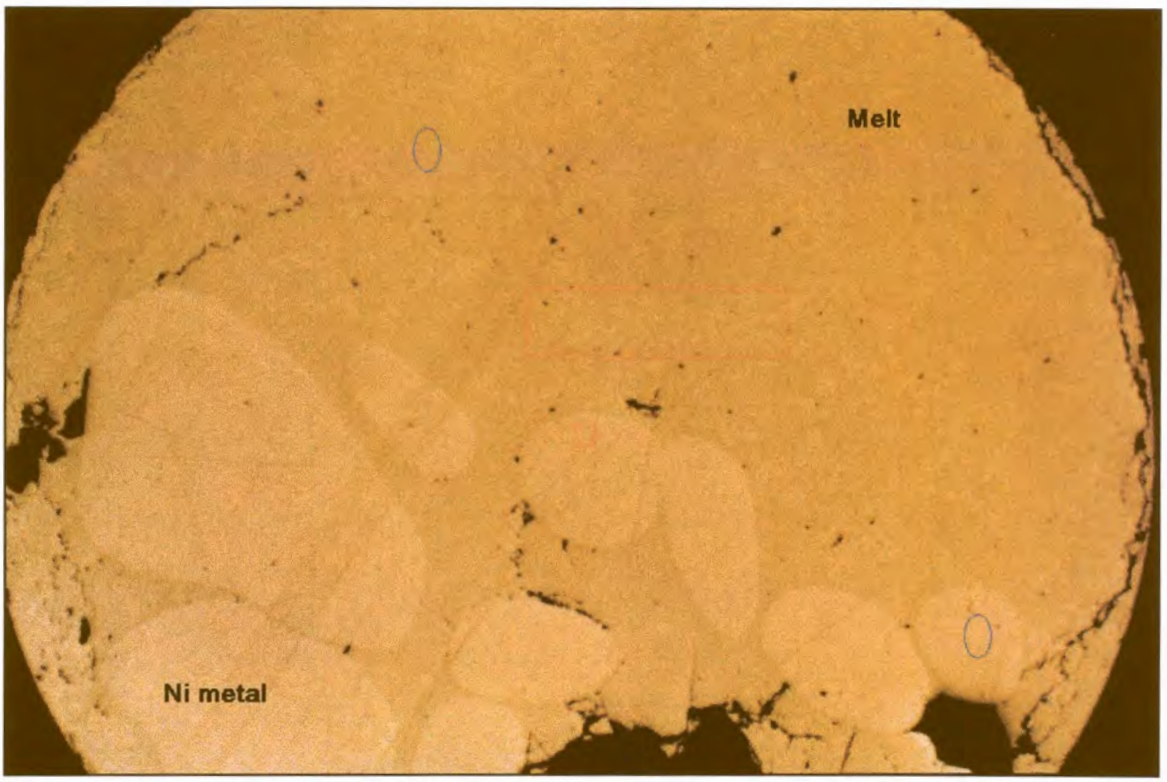

Figure 29. *Experiment HU429, co-existing nickel and quenched melt, equilibrated at 900°C. The red rectangles indicate the size and shapes of the areas analysed by micro-PIXE by moving the beam across the sample, and the blue ovals indicate the size and shape of the milli-PIXE spots, which are elongated to ovals due to the 45° angle of incidence with the incoming beam. Field of view 4 mm.*

In Figure 31 a calculated curve (yellow line) was fitted to the spectrum in Figure 30 with the GUPIX software, to quantify the elements. The background for the entire spectrum is very high, so that even the Ni and S peaks do not appear very clearly. If a huge amount of radiation of a certain energy reaches the detector, it is unable to handle the signal effectively and adds the signals so that a false peak at double the energy of the true peak is reported. This phenomena is called doubling and can be seen in Figure 30 for Ni and S. This same

effect described above also occurs at three or four times, or more, of the energy of the original peak, but with decreasing intensity. Two peaks – for example S and Ni – can also be added and a false peak created at the sum of their energies. This doubling or tripling also increases the background of the spectrum. The software package used to process the spectrum takes this effect into consideration. In Figure 31, the Pd and Rh-K peaks and the Pt L-peaks are mostly hidden by the high background, making accurate detection hidden by the S radiation. As Pt K radiation has a very high excitation energy, the L radiation has to be used for the analyses. impossible. The Rh and Pd L peaks are found close to the S K peaks, but are in this case

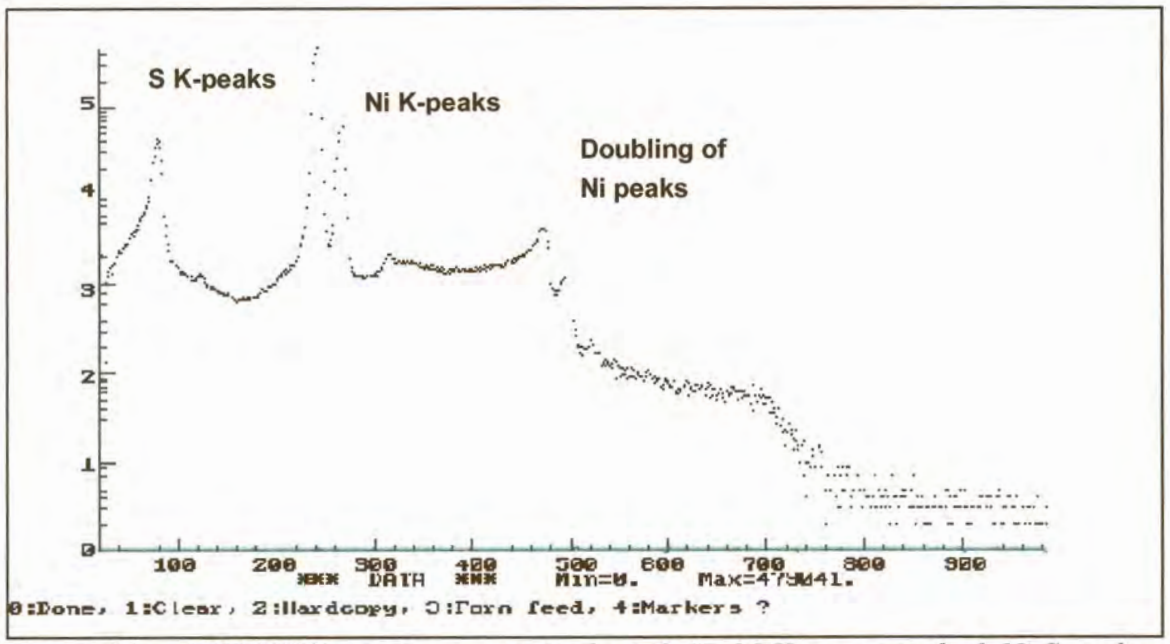

Figure 30. *Milli-PIXE spectrum acquired at 2.45 MeV on quenched Ni-S melt of experiment HU429, no filter. The vertical intensity scale is logarithmic. Doubling of the S peak, each Ni peak as well as the sum of the two Ni peaks and the sum of the Ni and the S peaks all increase the background.*

A spectrum acquired at the same spot as the spectrum shown in Figures 30 and 31, under the same conditions, but with a 125 µm thick Al filter inserted in front of the detector, is shown in Figure 32. The S peak visible in Figure 31 was completely removed from the spectrum, together with some of the Ni radiation. S is a light element and the Kα and Kβ peaks have low energies and are easily excitable, but are also easily absorbed. In this example, the background of the entire spectrum is lowered significantly, and the doubling

of the Ni peaks is also much reduced. This allows for accurate detection of the Pd and Rh K peaks by the software, although the Pd and Rh L peaks - located close to the S K peaks - were completely absorbed. The Pt L peaks remain difficult to detect, due to their position in the spectrum close to the Ni K peaks, where the background is very high. A thicker Al filter can be used to absorb higher energy radiation, and thereby to remove more of the Ni radiation from the spectrum and lower the background and Ni doubling further. However, a thicker filter would also absorb some of the Pt L radiation. The filter thickness has to be chosen to allow for optimum detection of the Pt peaks.

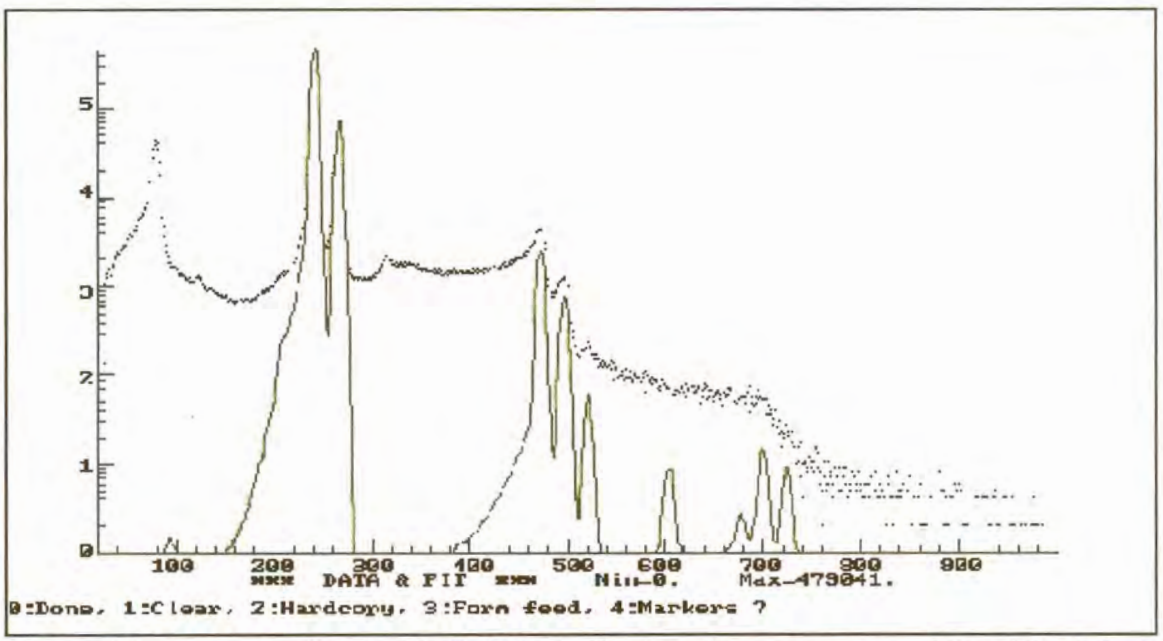

Figure 31. *Spectrum fitted with GUPIX (yellow) to determine composition. Fitted for Ni, Rh and Pd.*

The influence of the acceleration voltage was investigated by analysing the same spot on the Ni-S melt of experiment HU429, under the same conditions, first at 2.45 MeV and then at 3.00 MeV. The spectrum obtained at 3.00 MeV is shown in Figure 33 and can be compared with the 2.45 MeV spectrum in Figure 32. The peak to background ratio for the higher acceleration voltage is larger than for the lower acceleration voltage, making identification of Rh and Pd by the software possible, which was sufficient reason to perform further analyses at 3.000 MeV.

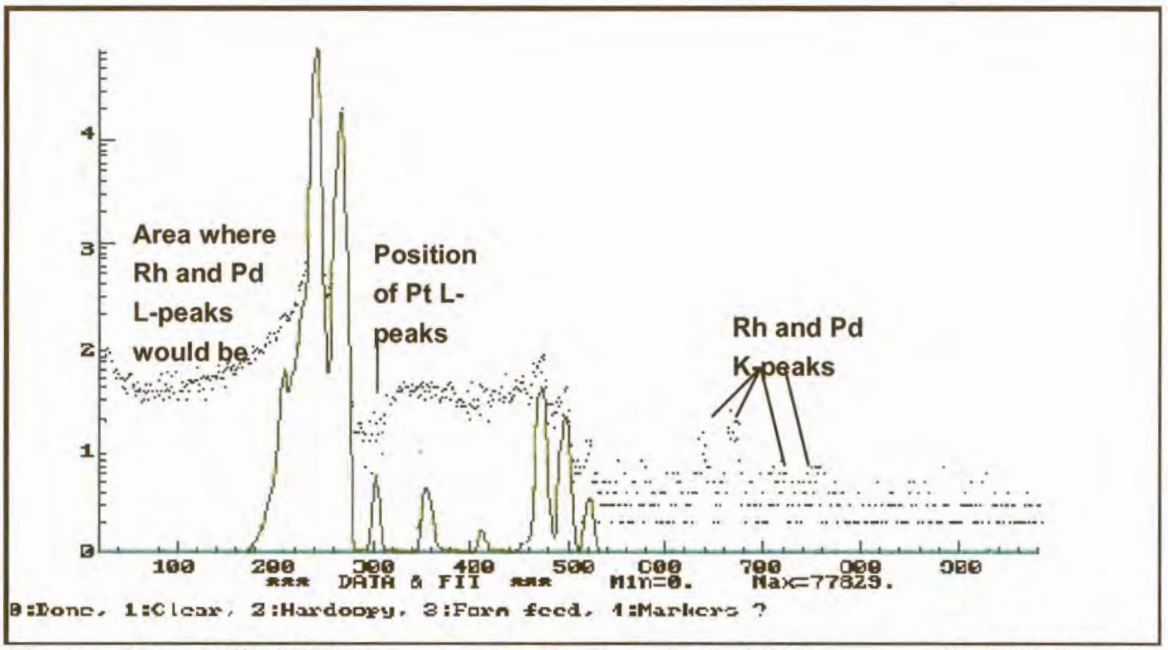

Figure 32. *Milli-PIXE spectrum acquired at 2.45 MeV on quenched Ni-S melt of experiment HU429, 125 μm Al filter.*

For the Ni-S system a 125 μm filter was used, and for the Fe-S and Cu-S systems a 200 μm thick filter was used (the Pt L peaks are even closer to the Cu and Fe K peaks than to the Ni K peaks) at an acceleration voltage of 3.00 MeV.

Analyses were generally left to collect $2x10^5$ counts on each spot. This took between one and three hours. Fewer counts did not provide spectra of the same clarity, and more counts usually did not improve the peak to background ratios significantly, due to an increase in the background. The beam current was generally between 0.2 and 0.7 nA, but was sometimes much lower due to technical difficulties. This did not have any effect on the quality of the spectra, only on the time it took to collect the spectra.

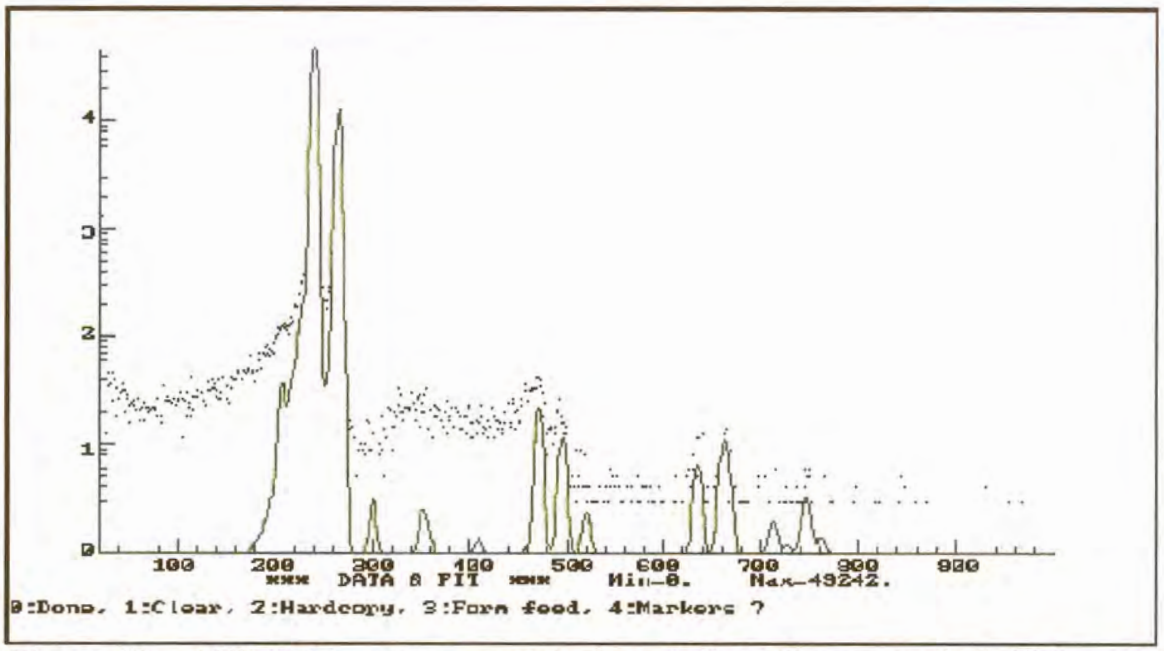

Figure 33. *Milli-PIXE spectrum acquired at 3.00 MeV on quenched Ni-S melt of experiment HU429, 125 μm Al filter.*

Table 6*. Evaluation of filter thickness and acceleration voltage.*

Acceleration voltage	Filter	Comment
2.45 MeV	None	Very high background - PGE below detection.
2.45 MeV	125 – 200 μm Al	Significant background reduction, almost complete removal of S radiation.
2.45 MeV	> 200 μm Al	Partial absorption of Pt L radiation.
3.00 MeV	125 – 200 μm Al	Slightly increased background, also increased peak to background ratio.

A spot that was analysed on Fe-S melt is shown in Figure 34. The carbon coating at the centre of the spot is discoloured. Analysis spots were always microscopically investigated to ensure that the correct positions were analysed. The size and shape of the milli-PIXE analyses are indicated in Figure 29, in comparison with the micro-PIXE analyses. Initially the spots were oval, but after the angle between the incoming beam and the sample surface was changed to 90°, the shape of the spot was round. The Fe-S analyses were performed with a round beam spot.

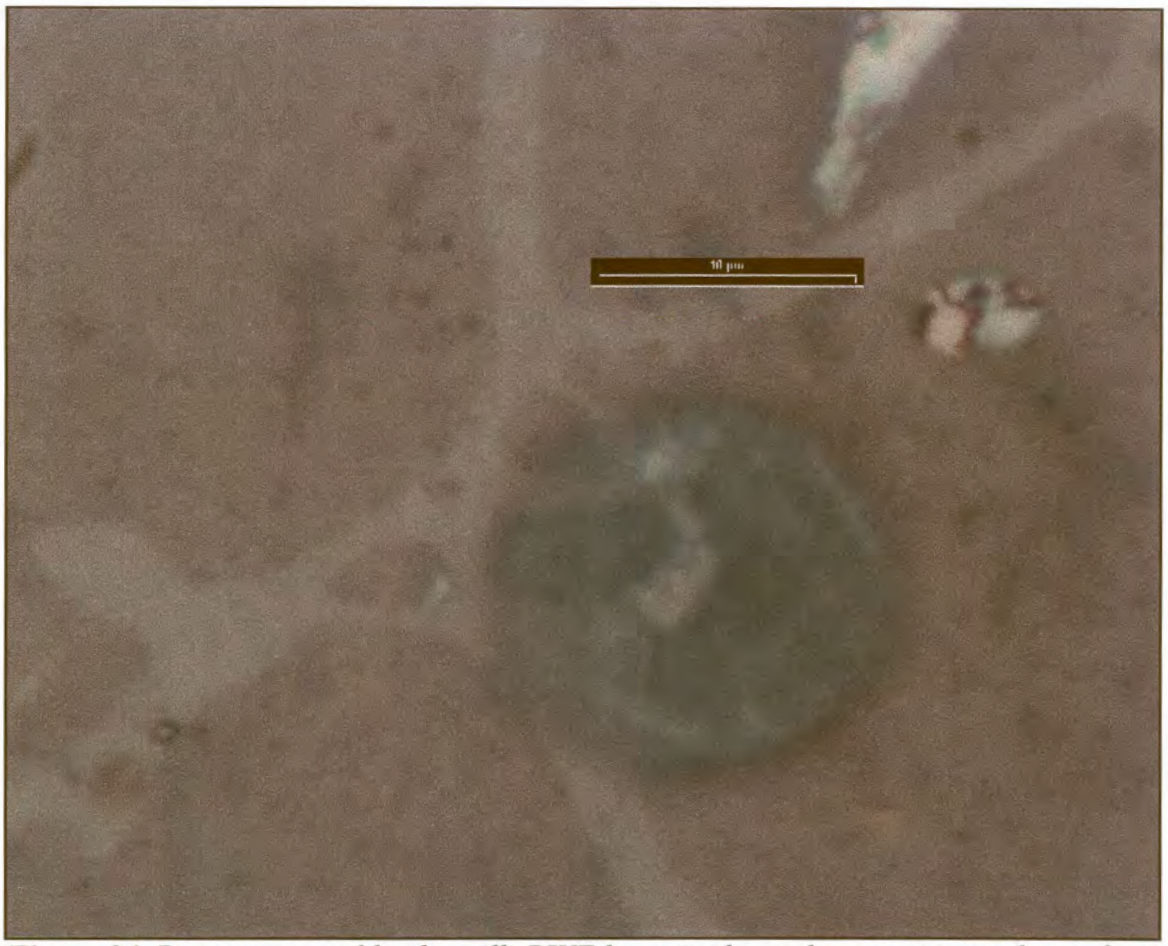

Figure 34. *Damage caused by the milli-PIXE beam in the carbon coating on the surface of Fe-S melt. The heterogeneous texture of the melt is visible. The scale bar is 10 µm. The diameter of the milli-PIXE beam is 100 µm. Only the central part of the beam caused damage.*

4.2.2. Micro-PIXE

At the National Accelerator Centre (NAC), a proton beam facility with a beam diameter of 2 µm is available, which allows PIXE analysis of microscopically small areas - called micro-PIXE. However, the quenched melts are heterogeneous, and larger areas were analysed to average out heterogeneities. This was achieved by rastering the beam over a rectangular surface on the sample while collecting the resulting X-rays. Typical areas analysed are indicated in Figure 29. A 125 µm Al filter was used to eliminate some of the major element radiation - mostly the S - to lower the overall background (as discussed for milli-PIXE, section 4.2.1.1.). A 3.00 MeV beam of H protons at a beam current of between 150 and 300 pA was used.

Whole spectra were collected until statistically acceptable peaks for the PGE were obtained, while noting the total counts. These were measured in nano-Coulombs (nC), and cannot be compared directly to the counts collected for the milli-PIXE analyses. Time varied from about 5 minutes to more than 10 hours per spectrum.

NAC data were processed with the GEOPIXE software described by Ryan *et al.* (1990). Yields and relative intensities are calculated, the X-ray spectrum is fitted by a least squares fitting routine and then combined with the yield calculations. EPMA major element analyses are incorporated with the PIXE data. Standard deviations and detection limits are determined individually for each element in each spectrum. The detection limits obtained for the PGE in each phase analysed are given in Table 7.

***Table** 7. Detection limits obtained for the PGE by micro-PIXE.*

Phase	Rh LLD (wt%)	Pd LLD (wt%)	Pt LLD (wt%)
Nickel	0.005	0.004	0.014
Ni-S-melt	0.0004	0.0005	0.001
Cu-S-melt	0.004	0.005	0.008
Digenite	0.0006	0.0007	0.002
Copper	0.009	0.011	0.032

4.3. Statistics

The averages (arithmetic means) and standard deviations were calculated from the EPMA analyses of each phase in the conventional way. Standard deviations are indications of the changes in instrumental conditions and heterogeneity of the analysed phases. Each individual PIXE analysis is supplied with an error calculated to reflect both counting statistics and peak overlap. As both EPMA and PIXE analyses values are accompanied by associated errors or standard deviations, these have to be considered when averages of the averages and ratios of the averages are determined. Resampling statistics were used in the

present investigation to make this possible, and to recalculate errors for the averages and ratios.

4.3.1. Resampling

Resampling is a Monte Carlo method that uses observed data to produce new hypothetical samples by randomly generating additional samples. Rather than using statistical formulae to describe a population, the technique simulates the underlying physical process. It is a useful tool for problems that require probabilistic and statistical analyses (Simon, 1997).

To determine the mean value of two or more means:
During the present investigation, mean compositions for phases had to be determined from EPMA analyses of several individual phases, each with its own mean and standard deviation (sections 5.1.1.1., 5.2.1.1., 5.2.2.1., 5.2.3.1., 5.3.1.1., 5.3.2.1., 5.3.3.1.). Several PIXE analyses of a specific phase, each with it's own associated error, were combined (sections 5.1.1.2., 5.2.1.2., 5.2.2.2., 5.2.3.2., 5.3.1.2., 5.3.2.2., 5.3.3.2.). This involves creating a normal distribution with a very large population according to the mean and standard deviation of each analysis. These populations are combined and a new mean and standard deviation obtained for the combined data. The larger the size of the recreated population, the more accurate the final values will be. The following routine was used.

MAXSIZE DEFAULT 15000	*Maximum sample size allowed.*
NORMAL 7500 (measured value1) (analytical uncertainty1) a	*Take 1 value from a simulated normal distribution with measured value 1 and analytical uncertainty1, and store in space "a". Repeat 7500 times.*
NORMAL 7500 (measured value2) (analytical uncertainty2) b	*Take 1 value from a simulated normal distribution with measured value 2 and analytical uncertainty 2, and store in space "b". Repeat 7500 times.*
CONCAT a b c	*Combine "a" and "b" and store in "c"*
MEAN c x	*Determine the arithmetic mean of "c", store in "x"*

STDEV c y	*Determine the standard deviation of "c", store in "y"*
PRINT x	*Print resampled mean*
PRINT y	*Print standard deviation*

To determine the mean of three or more values, values from simulated normal distributions of these values were also added to the resampled data, and included in the determination of the resampled average and standard deviation.

To determine the ratio of two means:

To determine partition coefficients, one population with a known mean and standard deviation was divided by a second population with known mean and standard deviation, to obtain a third population whose mean and standard deviation represents the ratio and its associated confidence interval (Section 6). The following routine was used.

MAXSIZE DEFAULT 15000	*Maximum sample size allowed.*
NORMAL 7500 (measured value1) (analytical uncertainty1) a	*Take 1 value from a simulated normal distribution with measured value 1 and analytical uncertainty1, and store in space "a". Repeat 7500 times.*
NORMAL 7500 (measured value2) (analytical uncertainty2) b	*Take 1 value from a simulated normal distribution with measured value 2 and analytical uncertainty 2, and store in space "b". Repeat 7500 times.*
DIVIDE a b m	*Divide population "a" by population "b" and store in "m".*
MEAN m x	*Store the arithmetic mean of "m" in "x".*
STDEV m y	*Store the standard deviation of "m" in "y".*
PRINT x	*Print the mean.*
PRINT y	*Print the standard deviation.*